Evaluation of various preprocessing techniques for classification of ultrasonic NDT signals

by

Kavi Ram Shahani

A Thesis Submitted to the
Graduate Faculty in Partial Fulfillment of the
Requirements for the Degree of
MASTER OF SCIENCE

Department: Electrical Engineering and Computer Engineering
Major: Electrical Engineering

Iowa State University
Ames, Iowa
1992

TABLE OF CONTENTS

LIST OF FIGURES

LIST OF TABLES

ABSTRACT

The integration of nondestructive test (NDT) methods into industrial environments has quickened in recent years as economic incentives to do so have increased. NDT methods find application both as a tool for inspecting manufactured goods as well as a tool for process control. Another important application involves the use of NDT techniques for detection of Intergranular Stress Corrosion Cracking (IGSCC) in nuclear power plant tubing. All these applications involve the analysis and interpretation of large volumes of data generated by transducers during the course of inspection. Techniques that can automate the process of analysis can contribute significantly towards improving both consistency as well as accuracy in interpretation.

One of the problems encountered in ultrasonic signal classification is the presence of temporal shifts. Consequently the transducer signal is preprocessed to extract features which are insensitive to temporal shifts. This thesis evaluates various preprocessing techniques in conjunction with neural networks for classification of ultrasonic NDT signals. Several preprocessing techniques were evaluated including the use of the Discrete Wavelet Transform. Alternate architectures such as the Time Delay Neural Network (TDNN) were also investigated. Results obtained to date demonstrate the potential of neural networks for performing complex classification tasks, and the importance of preprocessing techniques for successful flaw characterization.

CHAPTER 1

INTRODUCTION

Nondestructive testing (NDT) is a branch of materials science that is concerned with aspects of uniformity, quality and performance of materials and structures. Flaw detection and the interpretation of signals form a critical part of this interdisciplinary activity.

Nondestructive testing techniques are means by which materials and structures may be inspected without impairment of their performance. NDT techniques play a vital role in a variety of industries for evaluating the integrity of critical components. A typical NDT system [1] involves the use of a transducer for exciting the test specimen. The energy/specimen interaction is sampled by the receiving transducer. The received signal is then analyzed for evaluating the integrity of the test object. The diverse nature of NDT applications has led to the development of a variety of inspection techniques, employing different forms of excitation energy. Electromagnetic, radiographic and ultrasonic inspection techniques are a few examples. Of these, ultrasonic techniques are the most widely used method because of the simplicity and versality of the approach. Ultrasonic energy can propagate easily into the interior of many structures without excessive attenuation. Under appropriate conditions the returned signals carry sufficient information for determining important characteristics of the flaws in materials. A major aspect of research in ultrasonic NDT involves the analysis of received signals for classification of defects in the test object. The analysis is usually rendered difficult due to the

presence of noise and other artifacts present in the ultrasonic reflections [2].

One application of ultrasonic NDT is the inspection of heat exchanged tubes and pressure vessels in reactors. Process pipes and vessels are designed to have an added amount of metal wall thickness or a specific corrosion allowance based on conditions such as pressure, acceptable corrosion rates and the expected life of the equipment. Extremely high corrosion rates could lead to wall thining, resulting in dangerous conditions with regard to pipe and pressure ratings. If pipes and vessels become too thin, they could burst causing considerable plant damage. For this reason, in the particular case of nuclear power plant tubing, the ability to distinguish the ultrasonic reflections from intergranular stress corrosion cracking (IGSCC) is critical. Boiling water reactor (BWR) tubing is anchored with plates made of carbon steel at various intervals [3]. Over time, corrosion products at these junctures can cause cracks in the piping, which can lead to radioactive contamination of the cooling system. To avoid contamination, it is important to detect IGSCC as soon as it occurs.

The cracking usually occurs on the inside surface, close to the weld in heat affected zones. Detection of IGSCC by ultrasonic means is made difficult mainly due to the close resemblance of IGSCC signals to signals from nearby weld joint physical features, such as root welds and counterbores (ridges machined prior to welding to match unequal pipe wall thickness) as shown in Figure 1.1. Figure 1.2 shows a typical geometry. In order to use ultrasonic NDT method effectively, it is necessary to be able to discriminate between the naturally occuring features and flaw signals.

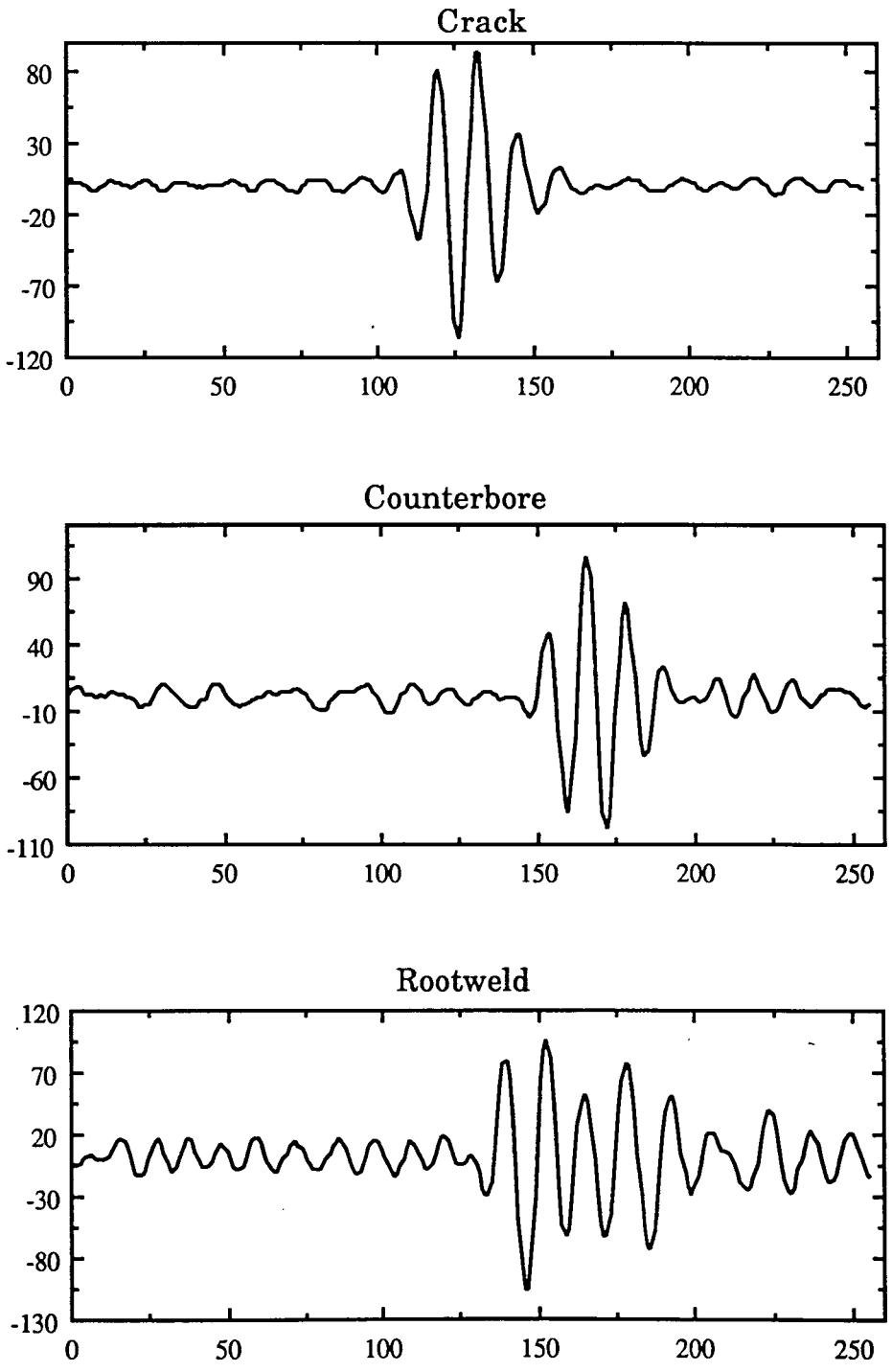

Figure 1.1 Typical ultrasonic signals

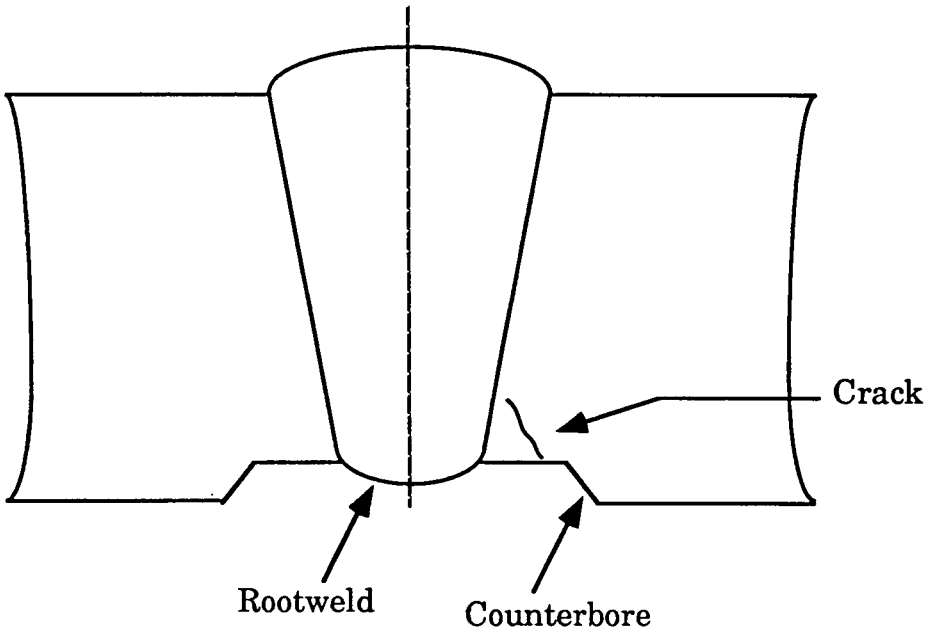

Figure 1.2 Geometrical relations between defects [2]

Presently such discrimination is performed by human operators who view the reflected ultrasonic signals on a CRT screen and use their experience and training to decide, whether or not a flaw is present. This thesis evaluates the application of various signal processing techniques for ultrasonic flaw characterization. The application of signal processing allows discrimination within an automated framework. The overall defect characterization scheme proposed in this thesis is shown in Figure 1.3. The first step in the classification process is preprocessing. The reflected

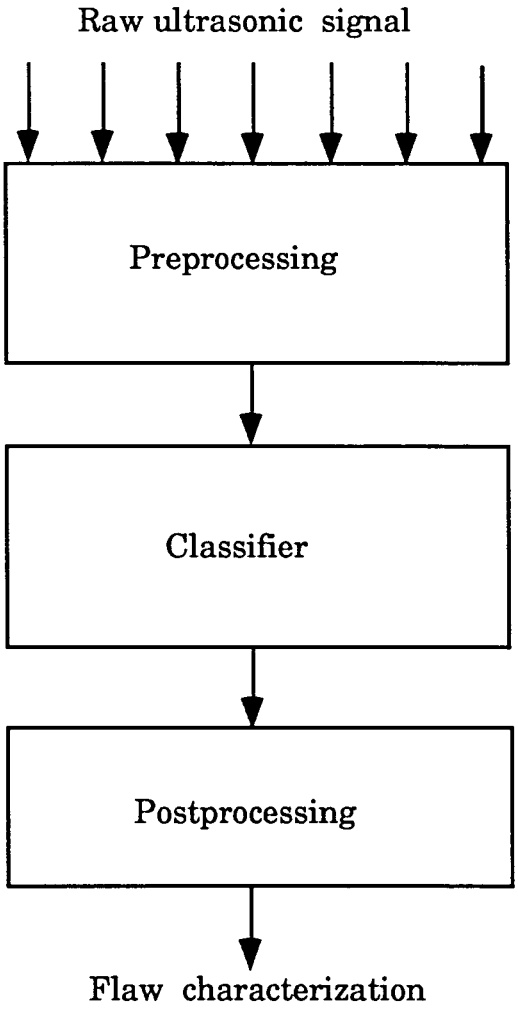

Figure 1.3 Overall classification strategy

ultrasonic signals contain information regarding the type, size and location of the defects. Defects are present at different locations in the material which result in temporal shifts of features in signals. The preprocessing stage renders the classification result relatively immune to effects of temporal variations in the signal. The preprocessing stage also compresses the information in the signal into a relatively small set of descriptors. Compression reduces the computational effort and minimizes problems caused by redundant information present in the ultrasonic signal. In this thesis, various preprocessing techniques, such as the discrete Fourier transform, the discrete cosine transform, the wavelet transform, are implemented in an attempt to ascertain the effectiveness of each method for ultrasonic flaw characterization.

The next step in the analysis process involves the classification of the signal. This thesis proposes the use of a multi-layer perceptron (MLP) neural network for classification, due to its ability to generate highly nonlinear decision surfaces in the multi-dimensional feature space. These networks do not require apriori statistical information about the defect signals. Alternate network architectures such as the time delay neural network are also investigated. The time delay neural network (TDNN) network is a variation of the multi-layer perceptron where a network of time delays is employed within the structure to identify features and their temporal relationships. As a result the network offers the advantage of invariance under temporal shifts in the signal.

In addition, distance measures such as the Euclidean distance and the Similarity coefficient are implemented to assess the effectiveness of

neural networks as pattern classifiers. A final postprocessing stage, is included to help reduce the error caused by ambiguous classifications.

Chapter 2 presents an overview of the concepts of ultrasonic nondestructive testing methods. A review of various signal processing techniques that have been applied to ultrasonic NDT waveforms, is given in Chapter 3. Chapter 4 introduces the concepts of neural networks and the architectures used for classification. Chapter 5 describes the contribution made by this thesis in terms of the evaluation of several signal processing techniques with respect to ultrasonic signal analysis. These techniques include the use of spectral coefficients, discrete cosine transform, cepstral analysis, envelope sampling, coarse coding, principal component analysis, and autoregressive modeling. In addition, the fundamental theory of the wavelet function and the wavelet transform method is developed. The results of applying the various preprocessing schemes to a database of ultrasonic signals are presented in Chapter 6. Finally, in Chapter 7, some conclusions, comments and areas for future research are presented.

CHAPTER 2

ULTRASONIC NONDESTRUCTIVE TESTING

Ultrasonic methods of examination have been used widely by industry for quality control and for determining the integrity of materials. The major advantage of using ultrasonic method of examination is the ability to detect both surface as well as subsurface defects. Ultrasonic techniques allow the detection and determination of the shape, size and location of flaws in materials. The technique can be employed in a number of other applications, including, for example, the measurement of thickness of sheets and pipes. A significant advantage of the method lies in the fact that it allows the examination of a variety of materials including metallic as well as non-metallic objects.

2.1 Wave Propagation

The ultrasonic inspection method makes use of mechanical waves [4]. These waves are composed of oscillations of discrete particles of material, although the particles themselves do not travel through the material. The energy produced forces the particles to vibrate progressively through the medium, from one plane to the next. The frequency (f) of a wave is the number of oscillations of a given particle per second. The wavelength (λ) is the distance between two planes in which the particles are in the same state of motion.

2.2 Modes of Propagation

There are several modes of ultrasonic wave propagation [5] namely the longitudinal (compression), transverse (shear), surface (Rayleigh), and plate (Lamb) waves. A brief description of each mode is given below.

Longitudinal waves occur when the displacement of the particles is in a direction parallel to the direction of propagation as indicated in Figure 2.1. They are most commonly used in ultrasonic testing because they are easily generated and detected. Longitudinal waves can travel through gases, liquids as well as solids.

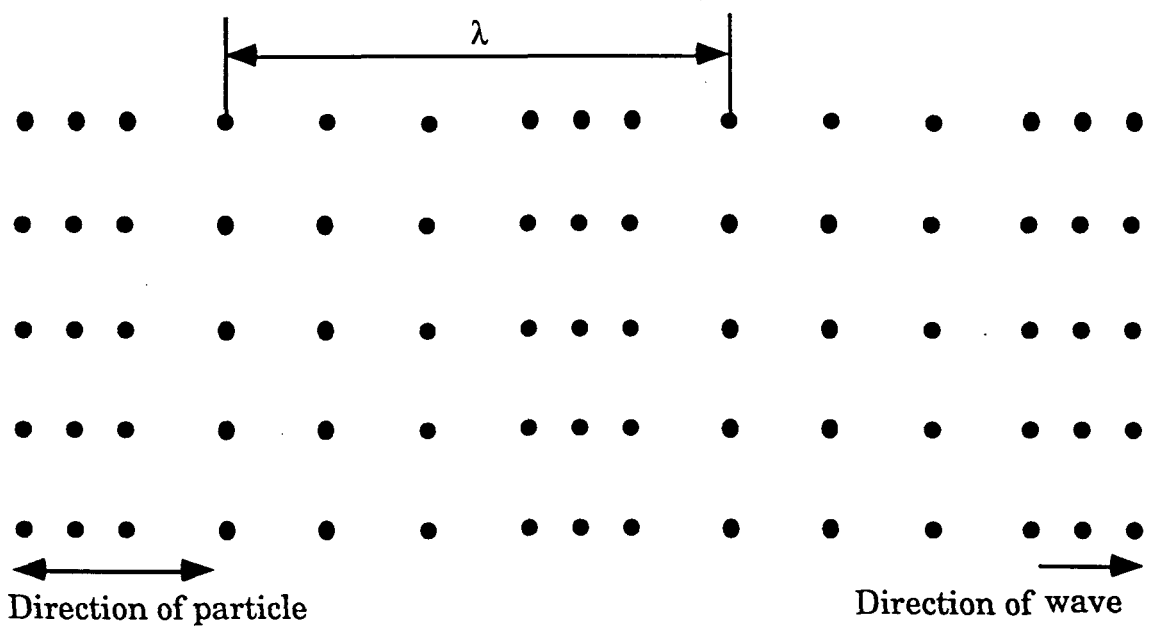

Figure 2.1 Longitudinal wave [4]

Shear waves occur when the displacement of the particles is transverse or at right angles to the direction of propagation as shown in the Figure 2.2. Shear waves travel at a velocity that is approximatley one half the velocity of the longitudinal waves in the same material. As a result, the shear wavelength is shorter than the longitudinal wavelength at the same frequency, making the shear wave more sensitive and more susceptible to scattering. However, shear waves can travel only through solids.

Surface waves are vibrations which propagate easily at the surface of the material. The amplitude of these waves decreases exponentially with depth attenuating to 0.37 of its maximum value within one wavelength.

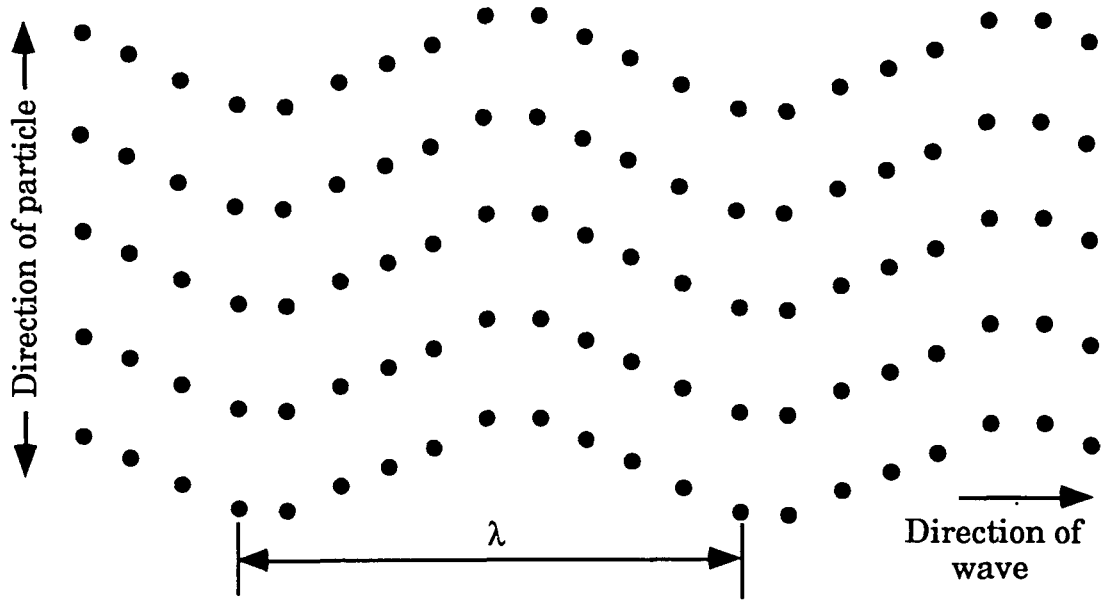

Figure 2.2 Shear wave [4]

The velocity of surface waves is approximately 0.9 times that of the shear wave and the particle displacement follows an elliptical orbit.

Plate waves are produced by ultrasonic vibrations in thin rods or plates whose thickness is less than or equal to a shear wavelength. Such waves occur in two different modes viz. symmetrical and asymmetrical [5].

2.3 Governing Equations

Ultrasonic fields in materials are governed by the elastic wave equation [6] having the form

$$\nabla . T + \underline{f} = \rho \frac{\partial^2 \underline{u}}{\partial t^2} \tag{2.1}$$

where $\underline{u}$ is the displacement vector. T is the stress tensor, ρ denotes material density and f represents the body force vector.

If we assume that

no body forces exist,

there are no internal losses,

the material is homogeneous and isotropic,

and the deformations present are small,

the field equation reduces to

$$(\mu+\lambda)\, \nabla\nabla . \underline{u} + \mu\, \nabla^2 \underline{u} = \rho \frac{\partial^2 \underline{u}}{\partial t^2} \tag{2.2}$$

The solution to equation (2.2), yields three orthogonally polarized plane wave solutions [7], one being the longitudinal wave and the other two, shear waves. Further, the velocity of the shear waves is approximately half of that of the longitudinal wave. As a result the direction of the group velocity is no longer parallel to the direction of phase velocity, so that the energy does not propagate perpendicular to the phase fronts [8]. Consequently the reflected signals tends to be corrupted by noise and artifacts, making the inspection of defects in materials a difficult task.

2.4 Acoustic Impedance

When an ultrasonic wave is incident on a plane boundary between two media, perpendicular to the surface, some ultrasonic energy is transmitted through the boundary and some energy is reflected back [9]. The fraction of energy transmitted and reflected depends on the specific acoustic impedance Z defined for each material as

$$Z = \rho V \tag{2.3}$$

where ρ is the density of the material and V is the velocity of the wave.

For two materials of different acoustic impedances Z_1 and Z_2, the percentage of energy transmitted, E_T, and percentage of energy reflected E_R, are given by

$$E_T = \frac{4 Z_1 Z_2}{(Z_1 + Z_2)^2} \times 100 \tag{2.4}$$

$$E_R = \frac{(Z_1 - Z_2)^2}{(Z_1 + Z_2)^2} \times 100 \qquad (2.5)$$

where $Z_1 = \rho_1 V_1$ in medium 1

$Z_2 = \rho_2 V_2$ in medium 2

2.5 Mode Conversion

When an ultrasonic beam is incident obliquely at an angle to the interface between two media having different acoustic impedances, the wave undergoes reflection and refraction, as shown in Figure 2.3. The angle at which the wave is reflected (α) is same as the angle of incidence. The angle of refraction (β), is determined by the sound velocities, V_1 and V_2 in the two media and the angle of incidence α as indicated in Figure 2.4. In general, when a longitudinal wave is incident at an interface, there will be three new waves created, namely a reflected longitudinal wave, a transmitted longitudinal wave and a transmitted shear wave. This phenomenon is known as mode conversion. Since different waves have different velocities in the same material, they will refract at different angles as shown in Figure 2.4.

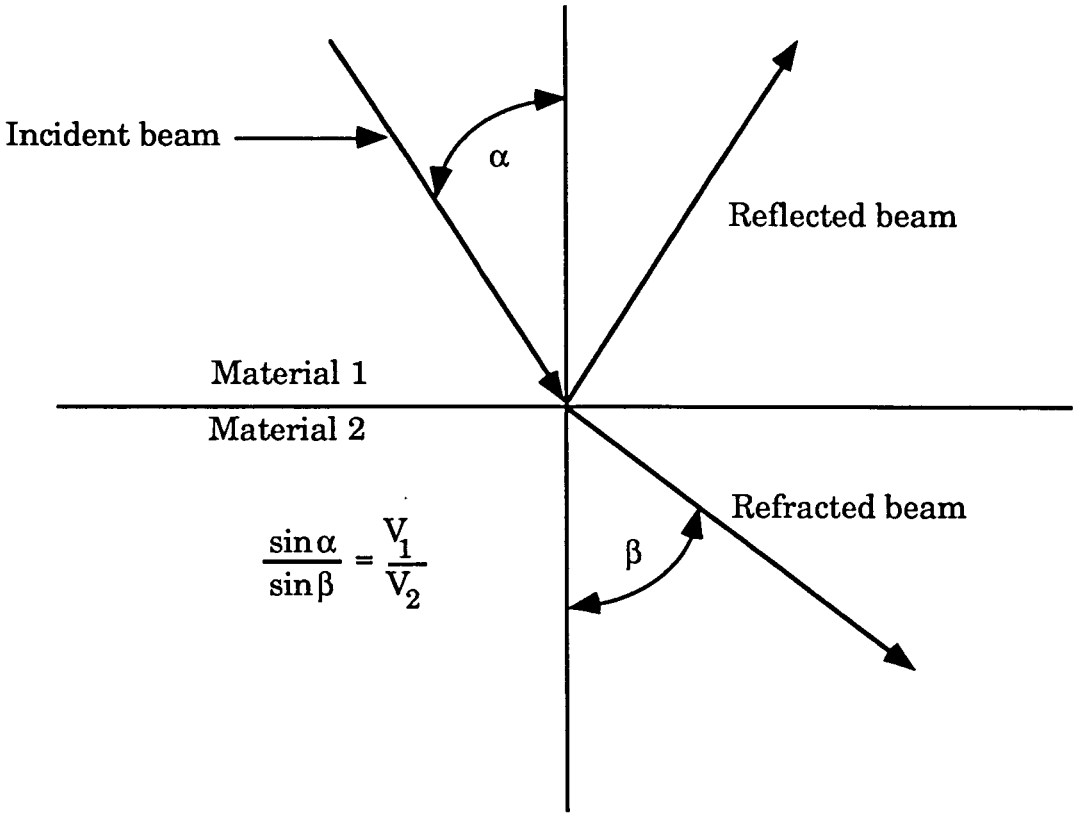

Figure 2.3 Reflection and refraction of a plane wave

2.6 Attenuation

The term attenuation is used to denote reduction in the ultrasonic intensity as the beam travels through the material. Attenuation of acoustical waves or signals is a consequence of two primary causes,

absorption and scattering. Absorption is the conversion of energy into other forms [5], such as heat. Scattering occurs due to the fact that the material is not homogeneous. Inhomogeneity can in general be due to a boundary between two materials such as coarse grain particles, pores and small defects. Ultrasonic scattering produces numerous echoes with different transmit times which result in artifacts, also known as grass or clutter, in which the true reflection is embedded.

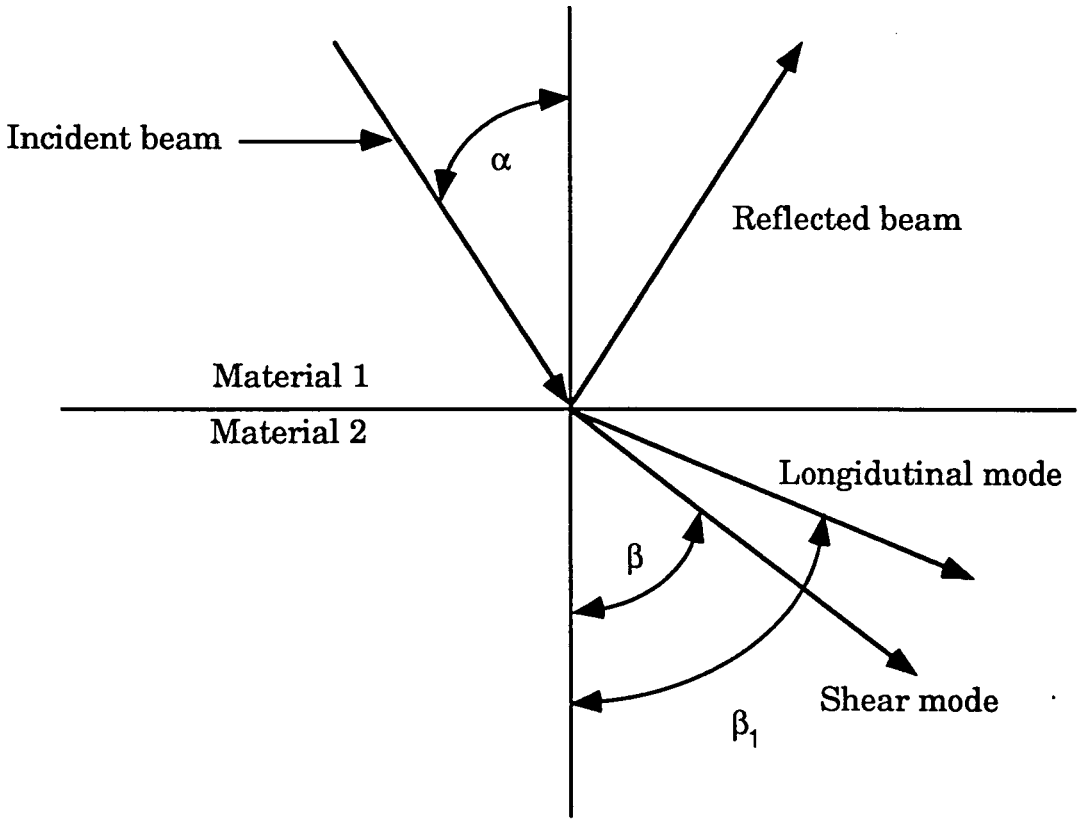

Figure 2.4 Mode conversion

2.7 Ultrasonic Transducers

Mechanical vibrations for measurement and analysis are generated by electromechanical transducers i.e. elements having the ability to transform electrical energy into mechanical energy and vice-versa. In most ultrasonic inspection systems, piezoelectric transducers are used. The active element in the transducer is a piezoelectric crystal which generates electric charges when mechanically stressed, and conversely, become stressed when electrically excited [10]. Such a material can be used as an ultrasonic transmitter as well as a receiver. The dimension of the piezoelectric element is nominally one half the wavelength at the center frequency of operation. It is placed between a backing element [7] for support and a wear plate for protection as shown in Figure 2.5. Some of the materials which exhibit piezoelectric effect include quartz, barium titrate, lead niobate and lithium sulfate. In order to provide a good contact between the transducer and the test material, a coupling material is utilized. The amount of energy reflected at an interface is given by

$$E_R = \frac{(Z_1 - Z_2)^2}{(Z_1 + Z_2)^2} \times 100 \qquad (2.6)$$

where $Z_1 = \rho_1 V_1$ in medium 1

$Z_2 = \rho_2 V_2$ in medium 2

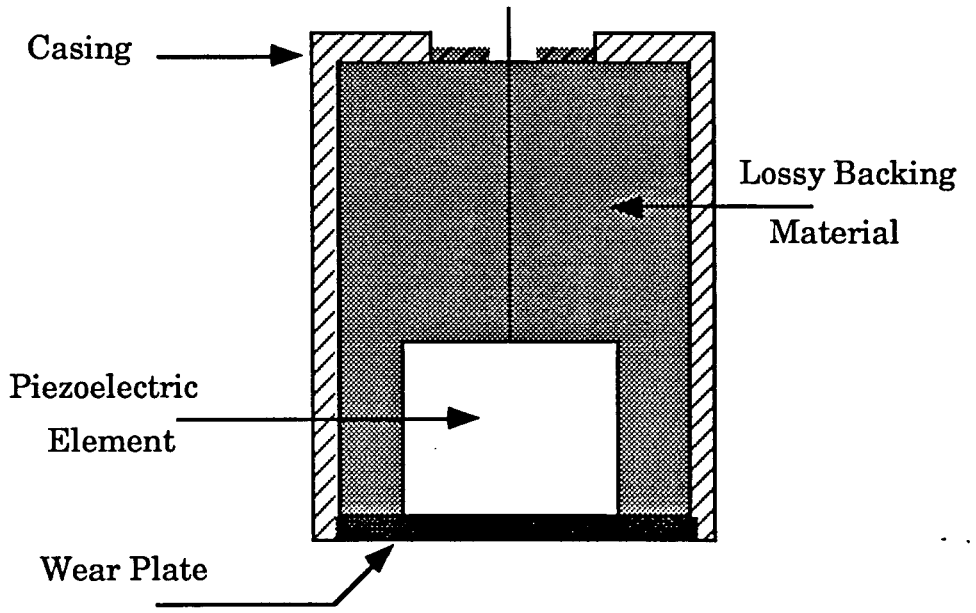

Figure 2.5 Piezoelectric transducer [11]

When $Z_1 = Z_2$, $E_R = 0$, indicating that all the energy is transmitted. Hence, smaller the impedance mismatch, greater the percentage of energy transmitted across the interface. Liquids such as glycerine, silicone, oil, water and grease serve as excellent transducer couplants.

Typically, a transducer operates when an electric pulse of short duration is applied to the crystal causing it to vibrate [12]. The excitation is allowed to decay after which the transducer is used in inverse mode to detect the reflected signal.

2.8 Test Methods

The active area of the transducer determines the amount of energy that can be transmitted into the test material [9,12]. The amplitude of the crystal vibration is small as a result of which a fluid couplant is used between the transducer and the test specimen. This type of testing is known as contact testing. In immersion testing, the sound is transmitted into the material through a water bath or liquid column. Figure 2.6 shows some of the configurations used for contact and immersion testing.

Contact testing and immersion testing are used in two modes, namely, pulse echo and pitch catch. The pitch catch technique uses two transducers, where one acts as a transmitter and the other as a receiver, as shown in Figure 2.6 (b), (c). The pulse echo technique uses a single transducer which operates as a transmitter in forward mode and as a receiver in inverse modes indicated in Figure 2.6 (a), (d).

2.9 Flaw Detection

Ultrasonic NDE involves the introduction of short bursts of high frequency elastic waves into a material [12,13]. By observing the resulting return echo it is possible to extract information about the material. The basic ultrasonic test system is shown in the Figure 2.7. The piezoelectric transducer is placed in contact with the material to be tested. The waves generated by the transducer travel through the material and are reflected

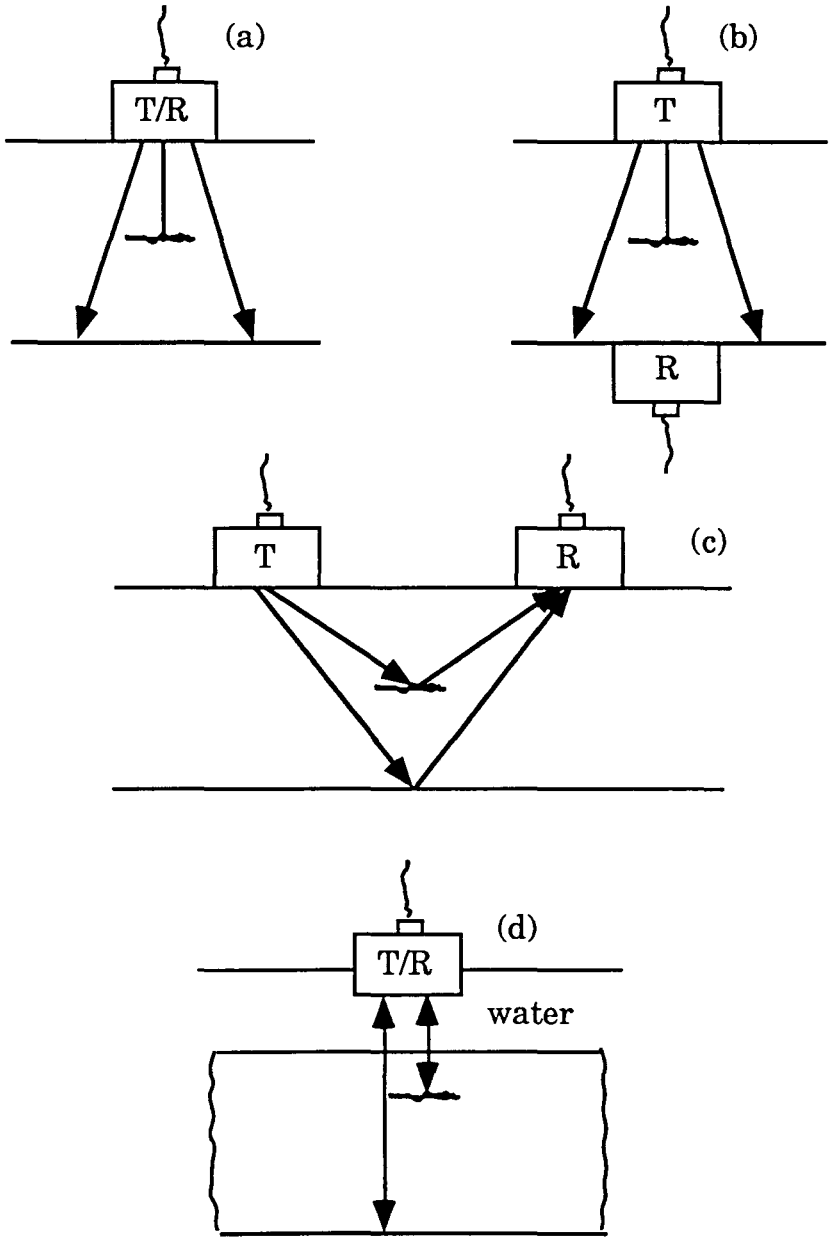

Figure 2.6 Basic configurations [15]

(a), (b), (c) Contact testing and (d) Immersion testing

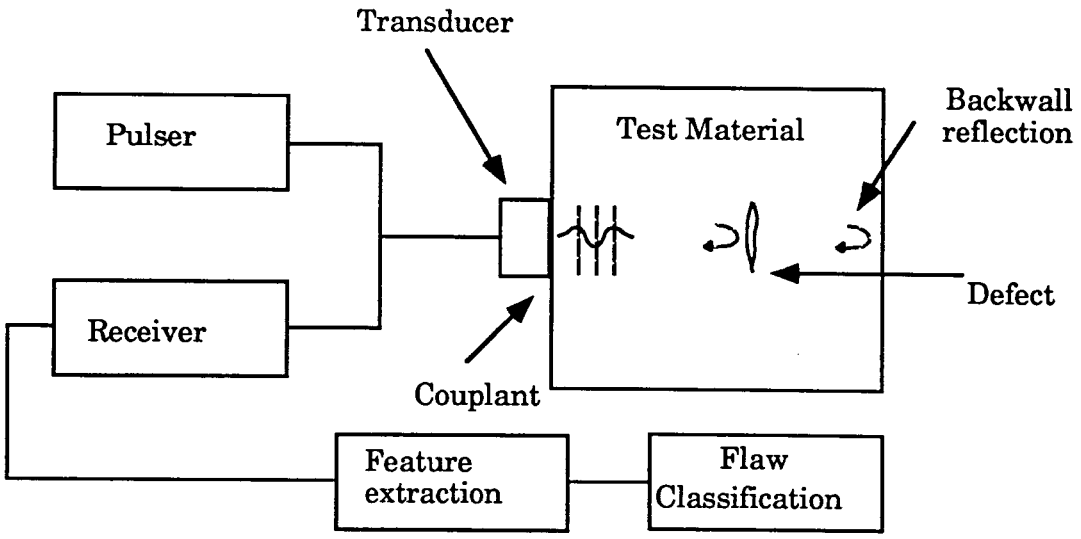

Figure 2.7 Ultrasonic test system [7]

or scattered by flaws in the material [11,13]. The reflected echoes are received either by the same transducer (as shown) or by a separate transducer placed in appropriate position on the test object. This information is then processed to extract relevant information, such as presence or absence of a flaw. This thesis evaluates various techniques for extracting such information from the ultrasonic signal.

A typical waveform of the received signal is shown in Figure 2.8. A flaw, if present, will be located between the frontwall and backwall reflection [14].

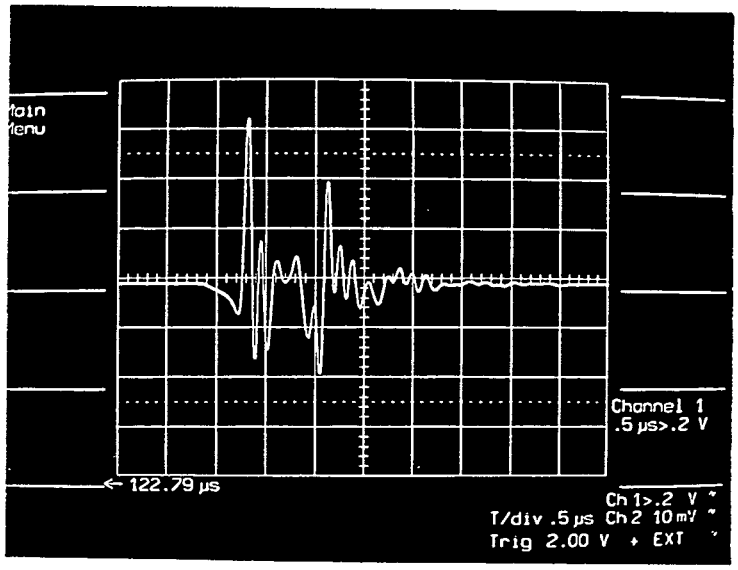

Figure 2.8 Typical ultrasonic reflection

Frontwall reflections are caused by the mismatch in impedance when the ultrasonic signal enters the test material and backwall reflections occur due to the mismatch in impedance when the ultrasonic wave exits the material. Care must be taken when sending the ultrasonic signal into the material so that signals from previous excitation do not interfere or overlap with the signal being observed.

The final component of the UT system involves signal processing and flaw characterization. The following chapters deals with the subject in greater detail.

2.9 Current Industrial Methods

The reflected ultrasonic signals are displayed using one of three types of presentation namely A scan, B scan or C scan as shown in Figure 2.9 [4]. In A scan echoes are displayed just as on an ordinary oscilloscope where the x-axis represents the distance travelled by the pulses and the y-axis represents the amplitude of the echoes. In the case of B scan, the probe scans the surface of the specimen along a line over time. The amplitude of the echos are displayed using the z-modulation of the cathode ray beam. The scan image represents a cross-section of the test

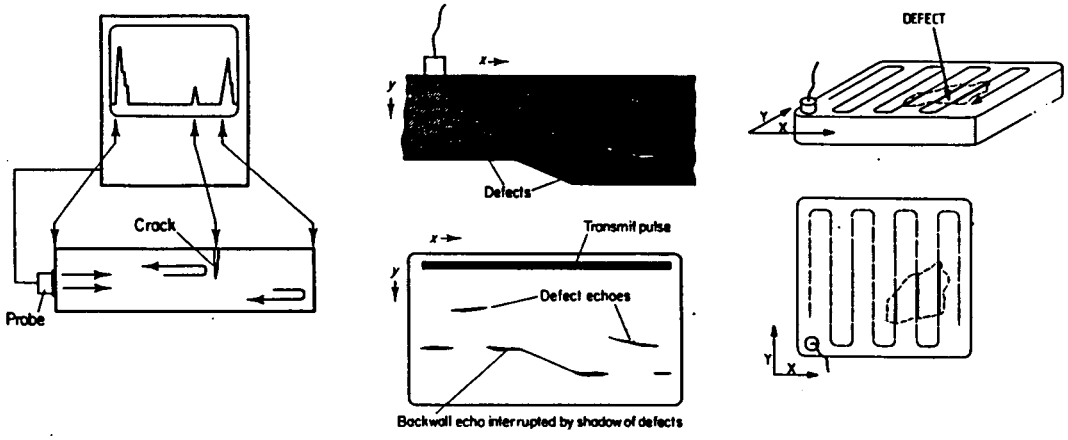

Figure 2.9 A scan, B scan and C scan [5]

object along the scan line of the probe. With a C scan representation, the display shows the flaw area as if it were viewed from above. For a C scan mapping, an X-Y scanner is used to translate the transducer in a plane

parallel to the test surface. This technique does not give any information with regard to the depth of the flaw between the top and the bottom surfaces of the test piece.

CHAPTER 3

DIGITAL SIGNAL PROCESSING AND FLAW CHARACTERIZATION

An importance aspect of research in nondestructive testing is defect characterization in materials. This has lead to the application of several digital signal processing techniques for enhancing inspection [16]. The aim of digital signal processing is to extract as much relevant information as possible from the reflected ultrasonic signals. In addition signal processing techniques are often used to compress information contained in the ultrasonic signal and format the signal into a form suitable for flaw classification. The processed ultrasonic signal is then analyzed for information leading to characterization of the flaw. This chapter presents a brief survey of techniques employed for extracting information about the shape, size and location of the defects.

The signals are usually interpreted from the displays of A or B scans. In practice, experienced and trained operators are needed to make the right decision. However, studies have indicated that the average human performance during inspection is much lower than an advanced, inspection system [17]. In addition, the performance of human beings depend on a number of factors [18,19], for example, operator boredom and fatigue were found to have a severe impact upon operator performance. Studies [17] have consistently indicated a need for automated inspection system. The following section present a brief overview of some of the methods employed for enhancing the quality of the signal.

3.1 Frequency Diversity Technique

The major difficulty encountered with an ultrasonic flaw detection system is the presence of microstructure noise (clutter) resulting from scattering at grain boundaries. Grain echoes exhibit randomness in amplitude and arrival time. One method of decorrelating grain echoes is by changing the frequency of the excitation signal [20]. This method is referred to as frequency diversity. Frequency diversity can be achieved by transmitting a broadband echo through materials and bandpass filtering the received echoes over many bands of frequencies. Flaw detection is sensitive to frequency diversity, and the outputs of the bandpass filters can be treated as a random vector representing information related to flaw and grain echoes. Saniie [20] used the statistical Bayes classifier design approach for flaw detection and grain-noise discrimination based on the information obtained from the output of bandpass filters.

The feature vector at any time t can be represented as

$$\underline{Y} = [y_1, y_2, \ldots y_k]^T \tag{3.1}$$

where each element y_i is the i-th filter's output signal, and k is the total number of filters used.

The Bayes classifier for flaw detection can be formulated as a sample problem in hypothesis testing where

Hypothesis H_0: Flaw is present

Hypothesis H_1: No Flaw is present

The Bayes classifier at a given time is represented by:

$$\phi(\underline{Y}) = \frac{p(\underline{Y} \mid H_o)}{p(\underline{Y} \mid H_1)} > \frac{P(H_1)}{P(H_o)} \text{ --> } H_o \qquad (3.2)$$

$$\phi(\underline{Y}) = \frac{p(\underline{Y} \mid H_o)}{p(\underline{Y} \mid H_1)} < \frac{P(H_1)}{P(H_o)} \text{ --> } H_1 \qquad (3.3)$$

where,

$\phi(\underline{Y})$ = likelihood ratio which serves as the discriminant function

$P(H_o)$ = probability of presence of flaw

$P(H_1)$ = probability of absence of flaw

$\frac{P(H_1)}{P(H_o)}$ = detection threshold

$p(\underline{Y} \mid H_o)$ = probability density function of flaw and grain echoes

$p(\underline{Y} \mid H_1)$ = probability density function of grain echoes

The use of a Bayes classifier requires a priori probability density function of each class. Saniie [20] assumes that the features from bandpass filters are normally distributed and vary about their means with different covariance

matrices. Hence, the probability density function of the feature vector is given by

$$p(\underline{Y},\underline{M}_i,\Sigma_i) = \frac{1}{(2\pi)^{\frac{k}{2}}}|\Sigma_i|^{\frac{-1}{2}} \exp[-(\underline{Y}-\underline{M}_i)^T\Sigma_i^{-1}(\underline{Y}-\underline{M}_i)], \quad i=0 \text{ or } 1 \tag{3.4}$$

where $\underline{M}_i$ is the mean vector and Σ_i is the covariance matrix of the input vector $\underline{Y}$. For a normally distributed feature vector it is more convenient to write the discriminant function in the logarithm form.

$$\log \phi(\underline{Y}) = \frac{1}{2}(\underline{Y}-\underline{M}_o)^T\Sigma_o^{-1}(\underline{Y}-\underline{M}_o) - \frac{1}{2}(\underline{Y}-\underline{M}_1)^T\Sigma_1^{-1}(\underline{Y}-\underline{M}_1) + \log\frac{|\Sigma_o|}{|\Sigma_1|} \tag{3.5}$$

The above equation represents a second order discriminant function. Assuming that the hypothesis H_o and H_1 are equally probable, the final decision rule is derived as

$$\begin{aligned} &\log \phi(Y) > 0 \quad \text{assign to } H_o \\ &\log \phi(Y) < 0 \quad \text{assign to } H_1 \end{aligned} \tag{3.6}$$

Figure 3.1 shows implementation of the technique.

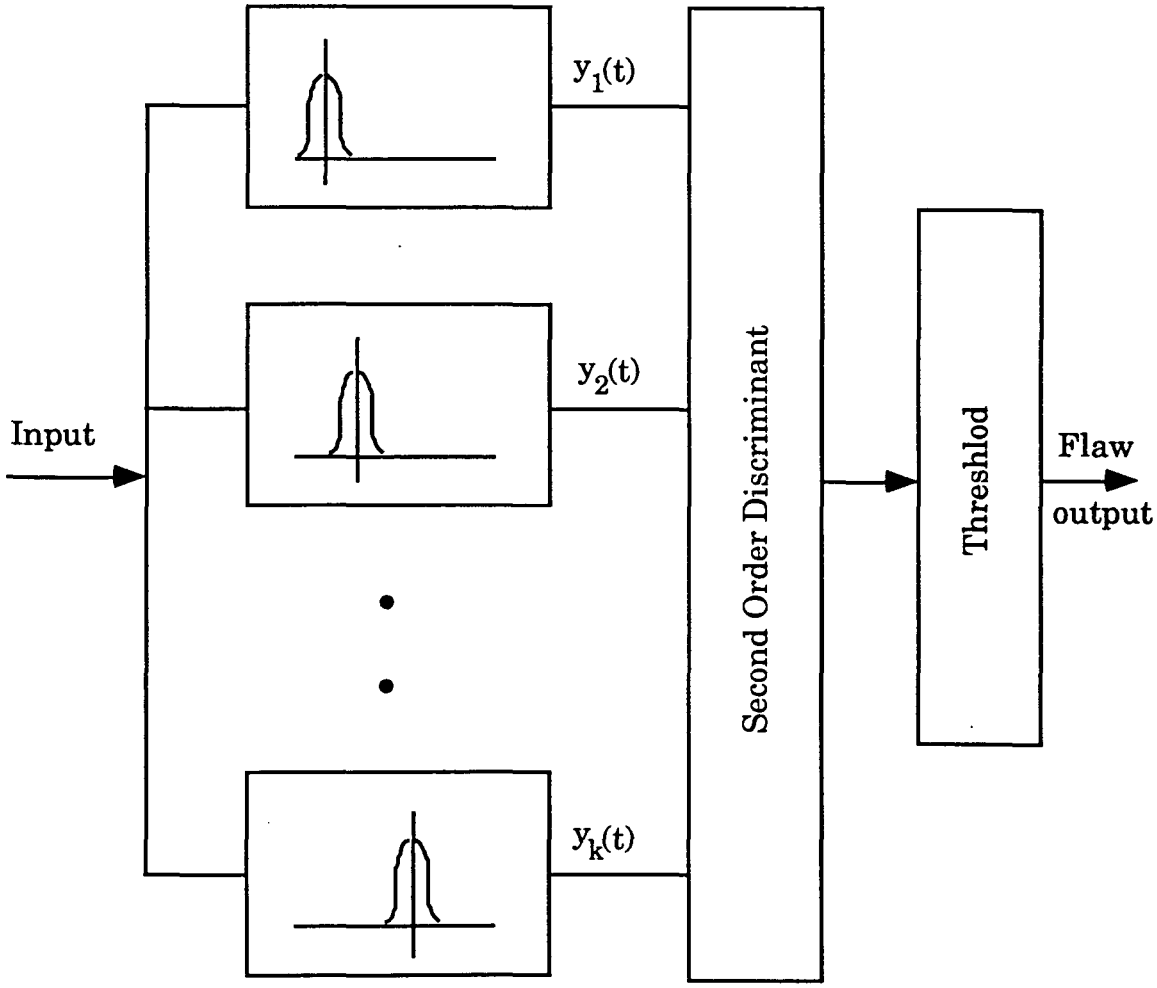

Figure 3.1 Frequency diversity technique [20]

3.2 Multiple Scanning Technique

Another method that eliminates the clutter noise is the spatial averaging technique. Lateral spatial averaging [11,21] assumes that the the lateral profile of the defects change gradually. If multiple scans of a single defect are taken in the lateral direction, similar to the B scan image and the results are averaged together, the random background noise is smoothed, allowing the flaw to be distinguished from noise.

Problems associated with this method include the requirement of apriori information concerning the flaw orientation and the assumption of uncorrelated noise.

3.3 Synthetic Aperture Focusing Technique (SAFT)

SAFT [22,23] is a signal processing method in which the ultrasonic wave measurements are used to generate a high quality image of a flaw. SAFT provides high resolution with a high signal to noise ratio using only a single transducer. The resolution of all imaging systems is limited by the effective aperture area i.e. the area over which data can be collected. Before synthetic aperture techniques were developed, the maximum aperture was limited by the ability to control the physical aperture used for data collection. The SAFT technique overcomes these limitations by synthetically creating large physical apertures. SAFT is a technique in which the focal properties of a large focused transducer are simulated or

synthesized by a series of measurements made using a small aperture transducer that scans over a large area.

The data are usually presented in the form of an unprocessed radio frequency (RF) signal or A-scan. Once the RF waveform has been recorded at one transducer position, also referred to as an aperture element, the transducer is moved to the next position and the process is repeated. Figure 3.2 shows the result of the process for 9 aperture elements.

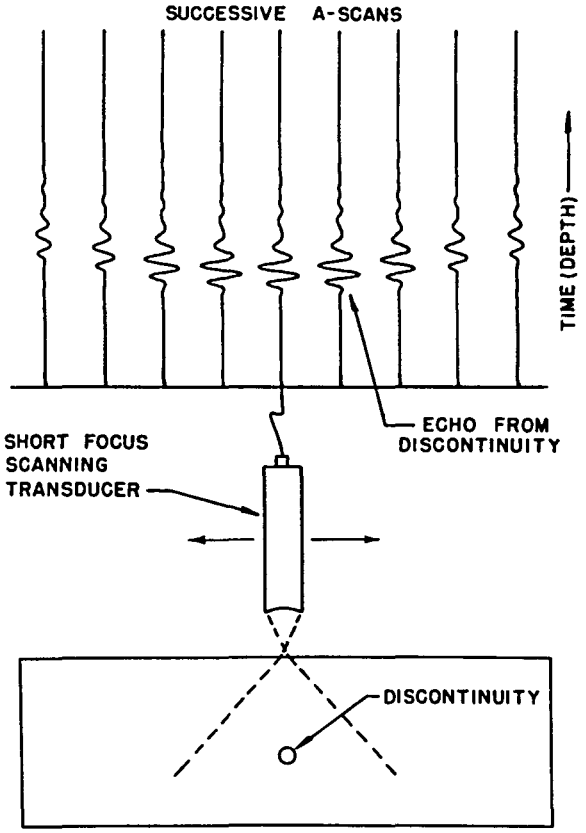

Figure 3.2 Synthetic aperture focusing technique (SAFT) [23]

The transducer in Figure 3.2 is focused above the test surface to produce a highly divergent beam. When the transducer is located directly above a discontinuity, the time delay is minimal. As the transducer moves away from this position, the time delay increases in a non-linear fashion.

The time delay between each transducer position and the defect is 2* distance/velocity. The factor 2 accounts for the fact that the pulse travels to the defect and back to the transducer. The distance R_{ijk} [24] between the i^{th} transducer position and the cell (j,k) can be expressed as (see Figure 3.3)

$$R_{ijk} = \sqrt{(\Delta Y+kdy)^2 + (\Delta X+jdx -ids)^2} \tag{3.7}$$

The distance is used along with the velocity to find the time of flight.

$$\text{time of flight} = 2\,R_{ijk}/\text{velocity} \tag{3.8}$$

Using the time of flight information, the amplitude of the recorded waveform S_i at a given point in time is summed into the image array at point (j,k). This is repeated for all N transducer positions. The summation for the intensity value at point (j,k) is given as

$$I_{ijk} = \sum_{i=0}^{N-1} S_i\left[\frac{2F_s}{\text{velocity}} R_{ijk}\right] \tag{3.9}$$

where F_s is the sampling frequency.

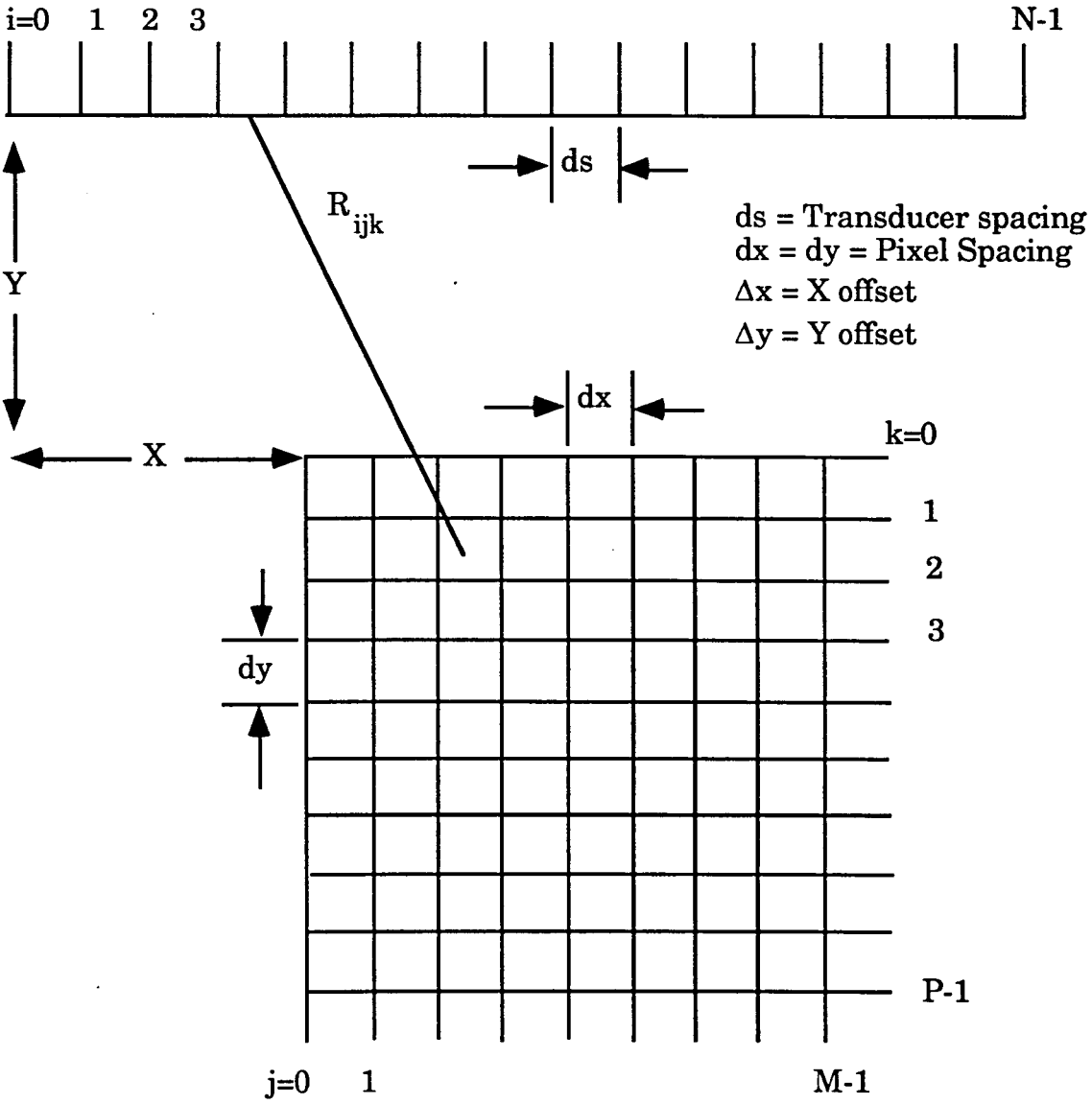

Figure 3.3 SAFT algorithm [24]

A major advantage of this waveform processing scheme is that the signal amplitude is substantially increased. Furthermore, the uncorrelated noise in each signal is almost completely eliminated. The enhanced ultrasonic signal is then used for extracting features which are, in turn, used for signal classification. Some of the methods commonly used for feature extraction are described next.

3.4 Feature Extraction

In order to render the flaw characterization system more efficient and reliable, selection of appropriate features is very important. The dimensionality of the measurement vector can be reduced by selecting only those features that contain discriminatory information. There are two important methods for selecting features. The first method known as optimum feature selection is based on maximization or minimization of a criterion function. The second method is called performance dependent feature selection. This method is related to the performance of the classification scheme, usually in terms of probability of classification error. The features selected are then input to the classifier.

Adaptive Learning Network is a feature reduction technique which is based on the second strategy. Brown [25] and Mucciardi [26] investigate the use of Adaptive Learning Networks (ALN) for the purpose of identifying flaws. ALN attempts to fit a polynomic model [27]

$$y = f(x_1, x_2, x_3, \ldots x_n) \tag{3.10}$$

where $x_1, x_2, x_3, \ldots x_n$ are the input variables and y is the output. The transfer function is built by employing a network of elements each of which computes a nonlinear function of a pair of input variables. Higher order multinomials can be generated by interconnection of the above elements. The input data set is partitioned into the training data and the testing data. Pairwise combinations of the input variables are fed to the first stage consisting of $m_0 = (n(n-1))/2$ modules as shown in Figure 3.4. The parameters or coefficient vector for each of the modules is then estimated. The testing data is then applied to the network and the best of the parameter vectors are chosen on the basis of an appropriate performance criterion exceeding a preset threshold value. The output of the m_1 ($<=m_0$) best modules forms the input to the next stage. The procedure is repeated and a set of m_2 ($<=m_1$) modules is chosen at the next stage. The process is continued until a single output is selected in the final stage. The overall transfer function is evaluated by back-tracking through the selected modules. Once the nonlinear model parameters have been identified, the nature of the flaw is identified either by observing the output synthesized from the selected list of input vectors or by using clustering algorithms in the multidimensional parameter space.

Doctor [28] uses the Fisher discriminant method to identify a small subset of features that contain the most amount of discriminatory information. In this method the n - dimensional data is projected onto a vector $\underline{W}$ described by the following equation as

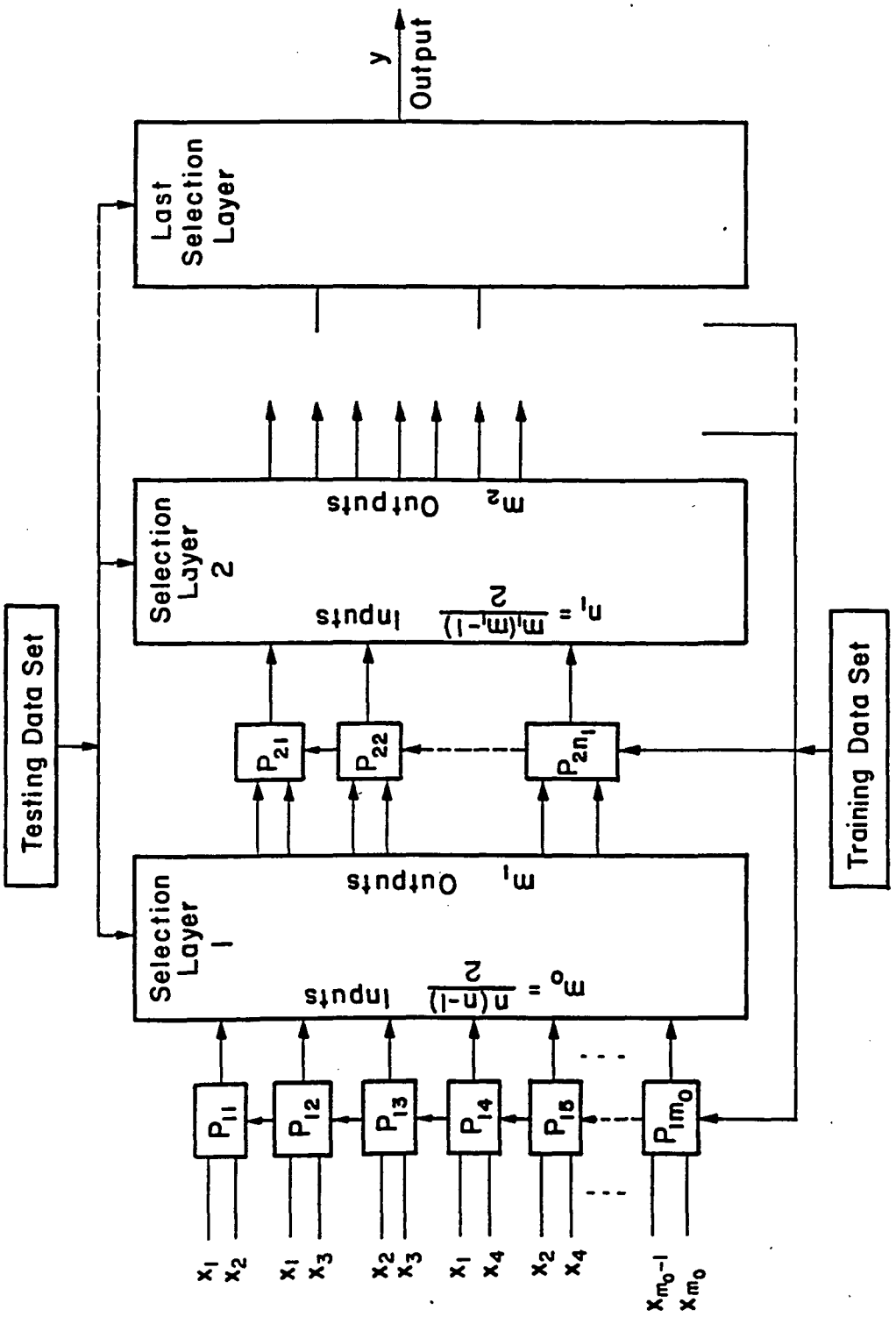

Figure 3.4 Block diagram of adaptive learning network(ALN) [27]

$$y = \underline{W}^T \underline{x} \tag{3.11}$$

where the pattern vector $\underline{x}_1, \underline{x}_2, \ldots \underline{x}_n$ have the corresponding projections $y_1, y_2, \ldots y_n$. If we consider a two class problem as shown in Figure 3.5 we would like to choose $\underline{W}$ so as to maximize the separation

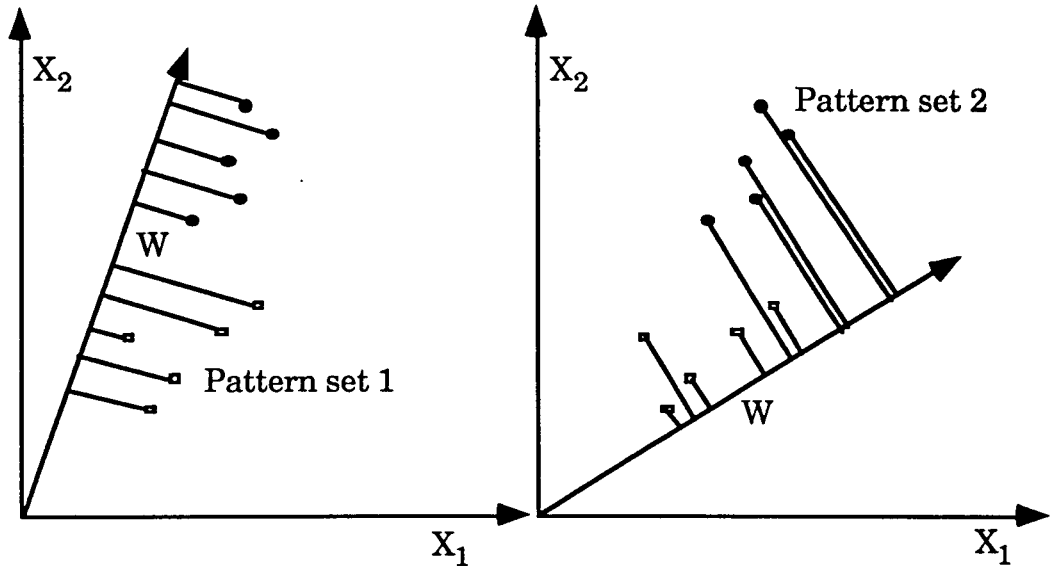

Figure 3.5 Fisher linear discriminant method

between the projections corresponding to the two classes. A quantitative measure of the class separability is provided by the Rayleigh quotient J which is a weighted ratio of inter to intra class "distance" between the patterns.

$$J = \frac{\underline{W}^T S_b \underline{W}}{\underline{W}^T S_w \underline{W}} \tag{3.12}$$

where S_b and S_w represent the inter class and the intra class scatter matrix respectively. The vector $\underline{W}$ which maximizes J is given by

$$S_b \underline{W} = \lambda S_w \underline{W} \tag{3.13}$$

If S_w is nonsingular then $S_w^{-1} S_b \underline{W} = \lambda \underline{W}$ which is a conventional eigenvalue problem. Classification using the projected data is obtained using standard pattern recognition methods . However, in much of the work reported in the literature features have been derived from raw time domain signal, frequency domain and spatial domain.

Rose [29] describes the use of three features namely rise time, pulse duration and the fall time to create a feature vector for classification. Classification is performed using the Fisher Linear Discriminant Method

Burch [21] computes features such as amplitude ratio, root-mean square variation of amplitude with angle, waveform pulse duration, waveform kurtosis, perpendicular deviation from best fitting plane and sphericity to form the feature vector. Classification was performed using the Fisher Linear Discriminant function.

Saniie [30] used LPC coefficients together with the resonating frequency and system poles. Actual classification was performed by finding the minimum Euclidean distance from a cluster center to a test vector.

CHAPTER 4

NEURAL NETWORKS

The increasing volume of information in various forms with different levels of complexities has lead to the development of sophisticated information processing systems. A major step associated with the design of modern information processing systems is automated pattern classification.

Pattern classification deals with classifying or labelling a group of objects on the basis of certain subjective requirements. Objects classified into the same class usually have some common characteristics. The classification requirements vary depending on the application problem. For example in recognizing the characters of the English language there are 26 pattern classes, whereas in distinguishing English characters from Chinese characters there are only 2 pattern classes. In order to accomplish this, a decision or discriminant function is necessary to partition the feature space appropriately.

The simplest approach for designing a pattern classifier is through the use of distance functions. This approach utilizes the concept of clustering in forming decision surfaces. Patterns with dissimilar attributes constitute different classes. The similarity of attributes can be measured in terms of functions such as the Euclidean distance and the Similarity coefficient.

A second class of pattern classifiers is based on an adaptive approach which relies on the process of training by means of an iterative learning algorithm. A typical learning algorithm involves presenting the classifier with training patterns of known classification. During the training phase, the classifier learns to associate the sample input patterns with their corresponding desired outputs. An example of such a type of classifier is the artificial neural network. Artificial neural networks are gaining increasing recognition as tools for solving problems of pattern recognition. Examples of applications include character recognition [31], process control [32], robotic control [33], speech recognition [34] and fault diagnosis [35]. The motivation and historical development of neural networks is described next.

Neural networks, also known as Parallel Distributed Processing (PDP) networks, connectionist models or neuromorphic systems, attempt to achieve good performance via dense connections of simple computational elements. They emulate the human learning process by attempting to mimic the human nervous system. This concept can be better understood by examining the human nervous system, and then comparing it to the characteristics of artificial neural networks.

4.1 Human Nervous System

The biological nervous system is a conglomerate of cells that continually receives information, elaborates and perceives the information, and then makes decisions. It does all this by means of neurons and

interconnections between neurons. It is estimated that the human brain is composed of 10^{12} nerve cells or neurons that can be classified into perhaps 1000 different types. Within each type there are many subtypes whose properties are defined primarily by their connections or their transfer functions. The complex function within the brain arises due to similar cells performing different functions depending on their connectivity. Figure 4.1 shows a typical nerve cell. The neuron or the nerve cell is composed of four regions [36,37]: the dendrites, the axon, the soma or the cell body and the presynaptic terminals of the axon. Dentrites of a cell are used to receive information from other cells. The axon on the other hand, is used to propagate information to dentrites of neighboring cells. The axon near its end, divides into fine branches, each of which has a specialized ending called the presynaptic terminal. The terminal contacts the receptive surface of other cells and transmits, by chemical or electrical means, information about the activity of the neuron to other neurons. The point of contact is known as the synapse. It is formed by the presynaptic terminal of one cell and the receptive surface of the other cell (postsynaptic cell). Within and around the soma are different types of ions such as sodium (Na^+), calcium (Ca^{++}), potassium (K^+), and chloride (Cl^-). When a voltage change is applied to stimulate the membrane of the soma, ions outside of the membrane are allowed to diffuse across the membrane and change the internal state of the soma. In other words, the neuron is excited by information received due to voltage change in the cell body. A neural network is formed by the interconnections of all the neurons via axons and dentrites, regulated by synapses. A neuron can be viewed as

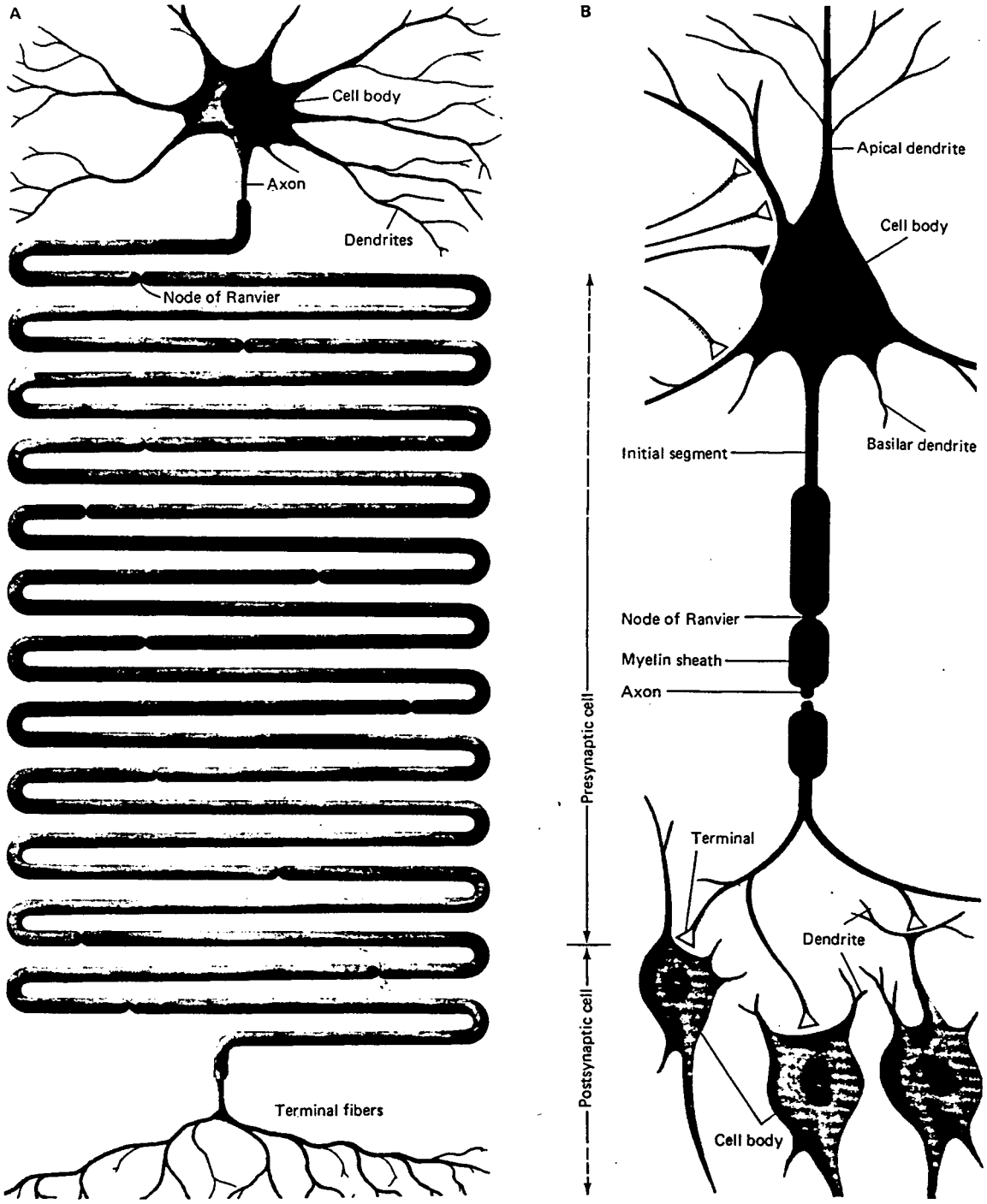

Figure 4.1 Typical nerve cell [36]

a processing element that produces an output only if the sum of the inputs exceeds a threshold level. The output signal is sent down the axon to other neurons and dentrites.

Artificial Neural Networks represent an attempt to mimic information processing strategy of the brain and therefore a lot of attention has been paid to the biological aspects of massively parallel realizations of intelligent activity. Before presenting the aspects of a neural network model, let us look at some of the features of the human nervous system.

1. Processing speed

The brain processes an element of information as much as 1 million times slower than the digital computer.

2. Processing order

Though, most advanced computers are able to process information one million times faster, the brain is a superior system for performing cognitive tasks. This is due to the order in which information is processed. The brain processes information in parallel where as conventional Von Neumann computers process information serially.

3. Abundance and complexity

It is estimated that about 10^{11} to 10^{14} neurons operate in parallel in the brain at a given moment. In order to emulate the activities in the brain, the artificial neural model will require a large number of processing elements. Therefore, practical implementations with current technologies would require some modifications.

4. Storage

Knowledge in the brain is thought to be stored in the interconnections between neurons. New information can be learnt or added by adaptation of the weights.

5. Fault tolerance

Brain has a much higher fault-tolerance than artificial neural systems.

6. Processing control

In the brain, each neuron has access to information contained only in those neurons to which it is directly interconnected. Therefore, the output of each neuron is a function of locally available information.

4.2 Artificial Neural Networks

Artificial neural networks [38] consists of a large number of simple processing nodes densely linked by interconnecting weights. The strength of the interconnection from one neuron to another is determined by its interconnecting weights. This is similar to the synaptic strengths in the biological case. Information is stored in the network in the form of weights and the scheme of weight connection therefore plays an important role in the network configuration. The nodes are often characterized by a nodal activation function as shown in the Figure 4.2. The nodal activation function sums up all the inputs from other nodes and determines whether the action is excitory or inhibitory. This models the activation potential in the cell body or the soma.

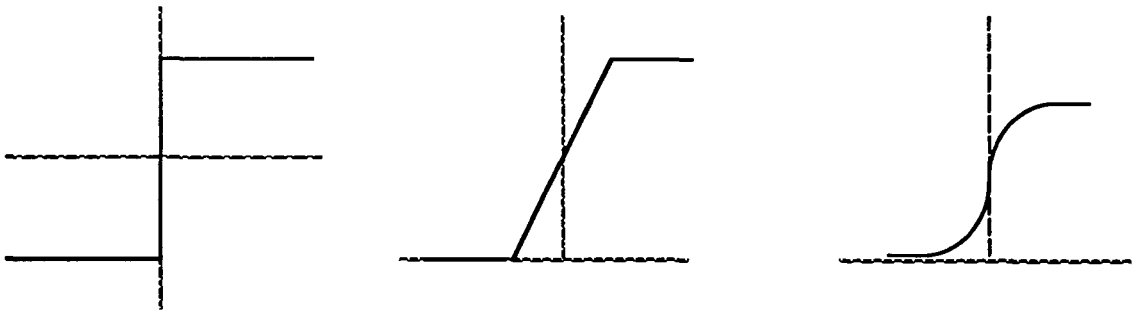

Figure 4.2 Nodal activations

Rumelhart [39] enumerates the eight major aspects of a PDP model.

1. Set of processing units.
2. State of activation.
3. Output function for each unit.
4. Pattern of connectivity.
5. Propagation rule.
6. Activation rule for combining inputs affecting a unit with its present state to produce an output.
7. Learning rule whereby interconnections can be modified on the basis of experience.
8. Environment within which the learning system must operate.

Although the mathematical modeling of artificial networks, are in general complex, a number of neural networks have been developed based on the eight concepts listed above. A taxonomy of six major classes of neural networks [38] are illustrated in the Figure 4.3. The networks are

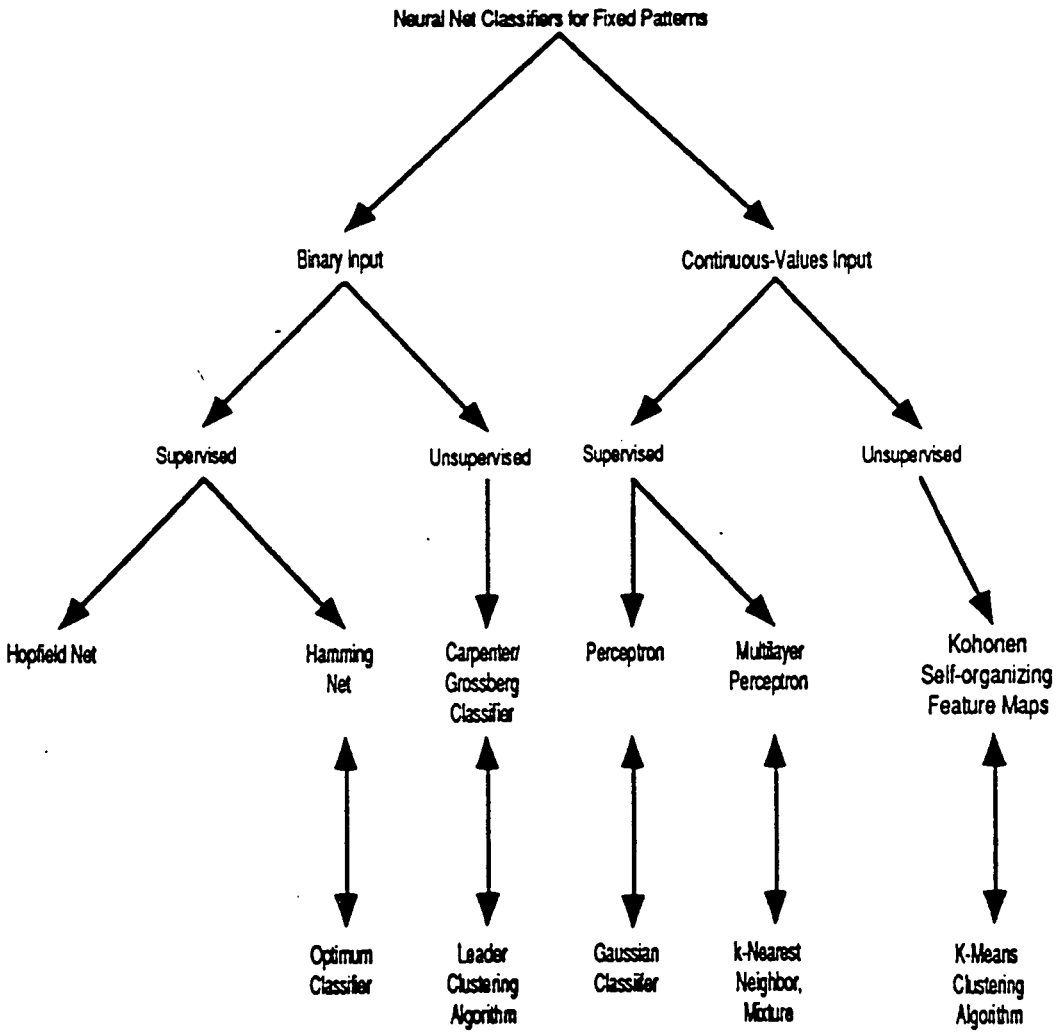

Figure 4.3 Taxonomy of neural networks [38]

divided into two classes that can operate on binary or continous valued outputs. They are further divided based on their training scheme which may be classified as supervised or unsupervised. Supervised training implies that the networks are presented with desired output during training process. The multi-layer perceptron employs supervised learning and finds widespread application in pattern classification. Unsupervised training provides no information of the correct class during training. Such nets, are used as vector quantizers to form clusters of the inputs. An example of unsupervised pattern classifier is the Kohonen's Self Organizing Feature Map [38]. The following section describes the multi-layer perceptron, network used in this thesis.

4.3 Multi-layer Perceptron

The multi-layer perceptron (MLP) are feed-forward networks with one layer of input nodes, one layer of output nodes and one or more layers of nodes between the input and output, called the hidden layers. Figure 4.4 shows a typical three layer MLP. Each layer in the network is fully interconnected to the adjacent layer by a weight structure. The use of additional hidden layers allows the generation of complex decision boundaries in the feature space. The ability to generate such surfaces is crucial in most pattern classification problems. Each node in the network is characterized by a nonlinear function, usually chosen as the sigmoidal function illustrated in, Figure 4.5. Figure 4.6, illustrates partitions which can be generated using the MLP [38].

In the standard MLP, the output of each node in the network is the nonlinear function of the weighted sum of the inputs connected to the node. When a large number of input nodes are used, it is usually necessary to normalize the weighted sum computed at each node so that the node operates on the linear portion of the sigmoidal function. Since a typical ultrasonic signal consists of 256 points, the MLP network used here was modified to ensure that the weighted sum at each node was within the linear range.

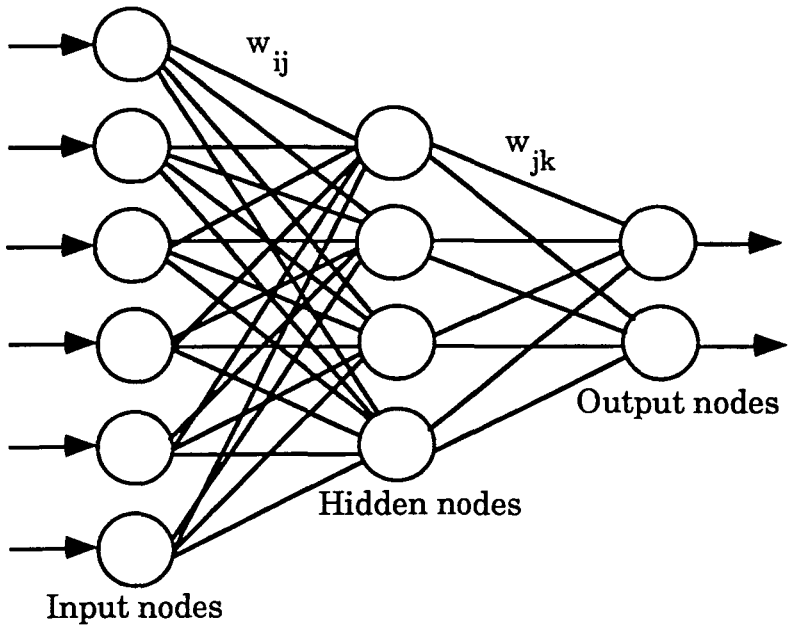

Figure 4.4 Multi-layer perceptron

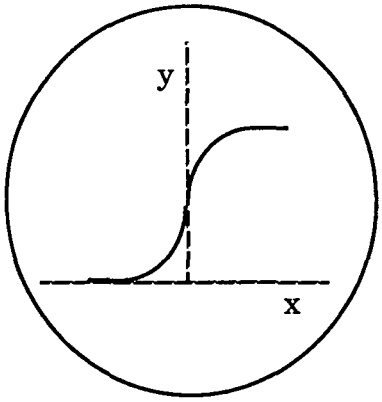

$$y = \frac{1}{1 + e^{-x}}$$

Figure 4.5 Sigmoidal activation function

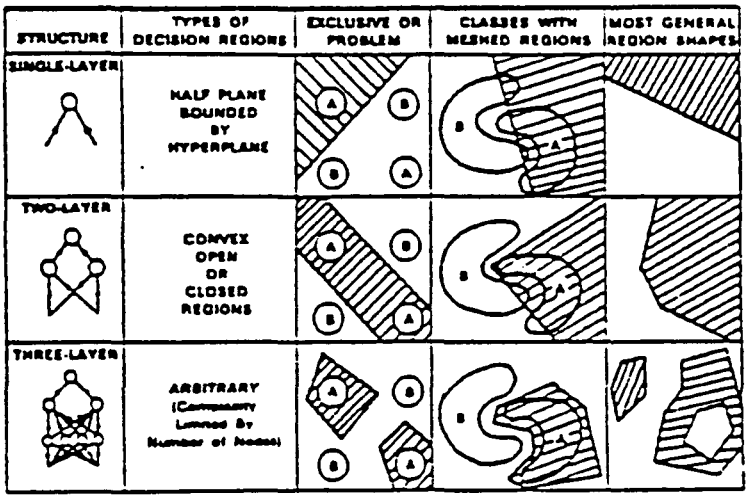

Figure 4.6 Surfaces generated by MLP [38]

The multi-layer perceptron operates in two phases namely the learning or training phase and the classification phase. One of the most commonly used training algorithms is the backward error propagation algorithm. The back propagation algorithm described in the next section has been applied to a number of deterministic problems, such as those related to defense [40], problems on speech synthesis and recognition [41], robotics [42], image processing [43], fault diagnosis [44] and target detection [45].

4.4 Backward Error Propagation Training Algorithm

The purpose of back-propagation algorithm is to determine a set of weights which when applied to an input vector, produces an output that is sufficiently close to the desired output. This is accomplished by using gradient search techniques for minimizing the mean square error between the actual output and the desired output. The mean squared error E is defined as

$$E = \frac{1}{2} \sum_{c} \sum_{j} (y_j - d_j)^2 \qquad (4.1)$$

where,

j is the output node index

c is the sample case index

y is the calculated output

d is the desired output

Training begins by applying patterns from known classes sequentially to the network. The mean squared error E is calculated and the weights are adjusted to minimize the error. Weight adjustment begins with the output layer and is propagated backward through the network. Hence, the name back-propagation. The algorithm cycles through the training data repeatedly until the network is trained. A single pass through the entire training data set is called an epoch. The network is considered trained when the error between the actual and the desired outputs falls below a certain threshold, or until a given number of iterations has been exceeded. The steps involved in the back-propagation is presented below:

1. Initialize weights to small random values.
2. Present an input vector to the input nodes and the corresponding output to the output layer of nodes.
3. Calculate the actual output values corresponding to the input vector presented to the network in step 2.
4. Recursively adapt weights starting at the output nodes and working back to the input using the equation:

$$w_{ij}(t+1) = w_{ij}(t) + \eta\delta_j x_i \qquad (4.2)$$

where $w_{ij}(t)$ is the weight connecting node i to and node j, x_i is either the output of node i or an input to a node j, η is the learning rate. The term δ_j

represents the error associated with node j. If j is an output node, then we have

$$\delta_j = y_j(1-y_j)(d_j - y_j) \tag{4.3}$$

If the node j is in the hidden layer, then

$$\delta_j = x_j(1-x_j)\sum_{<k>} \delta_k w_{jk} \tag{4.4}$$

where k is over all the nodes in the layer above node j.

5. Repeat by going to step 2 until convergence is achieved.

The derivation of the equations for backward error propagation training algorithm is presented in Appendix A.

4.5 Convergence Issues

A major drawback of the back-propagation algorithm [46,47] is that it suffers from problems usually associated with gradient techniques, namely, convergence to local minima and lack of convergence due to oscillations between two points. Figure 4.8 explains the above situation.

In this one dimensional example, initial weights w_a and w_b will converge to local mimina whereas w_c will converge to the global minimum. As a result, back propagation performs poorly in cases where more than one minimum is present. In addition, it is possible that the weights will

oscillate between two points and fail to converge, as in the case at points w_d and w_e in Figure 4.8.

The wide range of applications of the back-propagation algorithm and the multi-layer perceptron has resulted in an extensive analysis of the method. This has led to several interesting areas of research such as hidden layer optimization [48], learning rate improvement [49,50], alternate connection topologies [51,52] and alternate threshold functions [53]. The MLP is sensitive to temporal variations in the input signal. Temporal variations in ultrasonic signal arise due to varying flaw depths and flaw locations. The time delay neural network described in next has the advantage of being insensitive to temporal variations in the input signal.

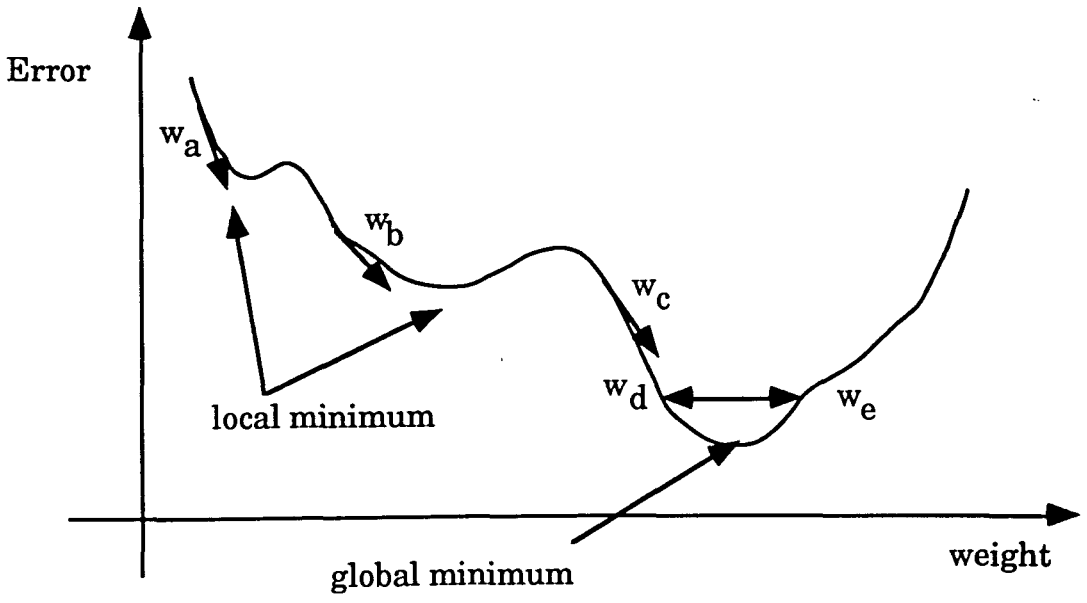

Figure 4.8 Convergence of back-propagation [47]

4.6 Time Delay Neural Network

The time delay neural network (TDNN) closely resembles the multi-layer perceptron with the added advantage of being insensitive to temporal shifts in the input signal. This is an important property, particularly since flaw classification is to be performed independent of the location of the defect in the test object.

In MLP, the basic unit computes the weighted sum of its inputs and then passes this sum through the sigmoidal function. In case of the TDNN, the basic unit is modified by introducing delays D_0 through D_N [54] as shown as in Figure 4.9, where D_0 represents the undelayed signal and D_i i=1,2 . . N represent a delay of i time units. The J inputs of such a unit are multiplied by a set of weights for each delayed version.

The TDNN therefore has the ability to correlate the features in the input signal and exploit their temporal relationship. An alternate interpretation is to consider each hidden unit as connected to a slice of the input vector, and the slice or window is moved down the input vector in unit steps. This can be explained with the help of Figure 4.10.

The network shown consists of n rows, each containing m hidden units connected to m successive slices or receptive fields of the input vector. The m weights connecting the hidden units of a given row to m successive input units are put in one class. The TDNN is trained using the back-propagation algorithm with the added constraint that the weights to all the time-shifted versions remain the same [55]. At the end of each iteration,

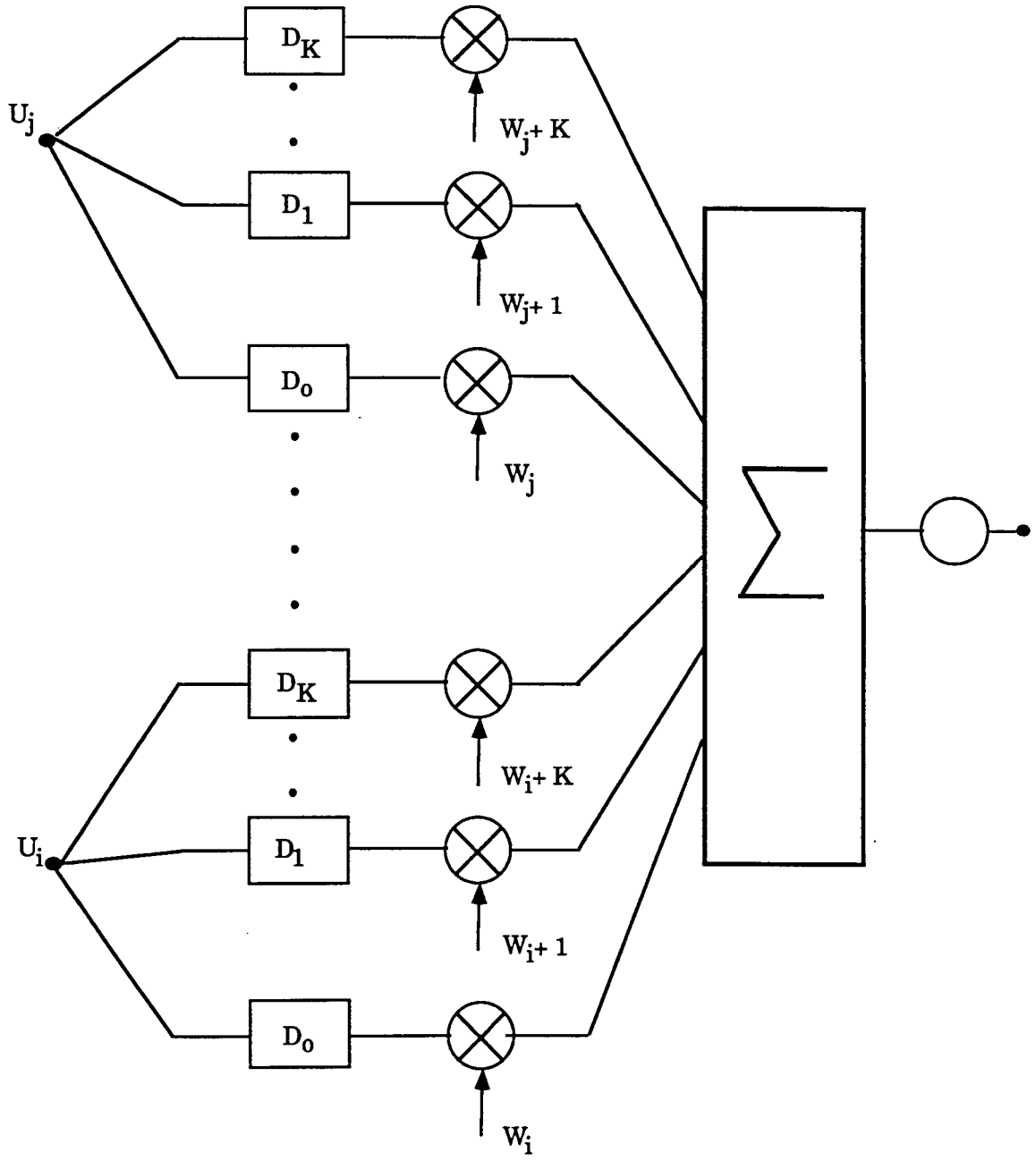

Figure 4.9 Basic TDNN unit [54]

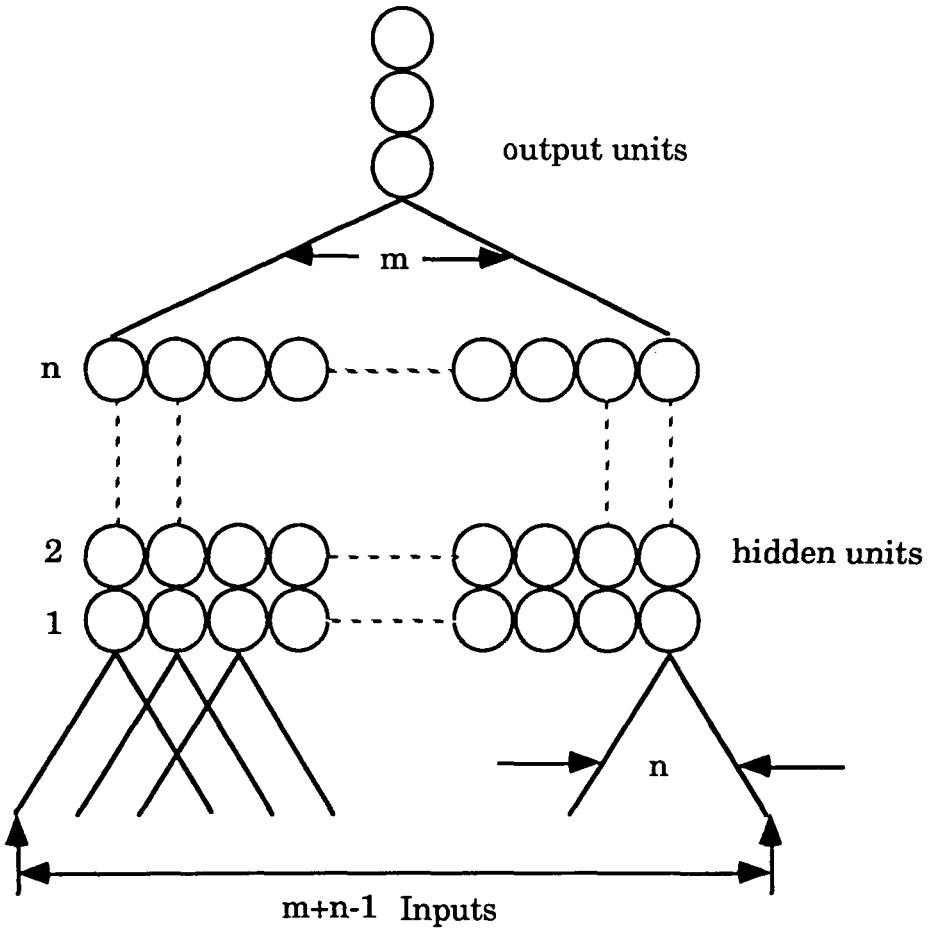

Figure 4.10 TDNN representation [55]

where the weights are updated, every weight in an equivalence class is set to the average of the weights in that class. This enables the network to extract position independent features from the input signal. As a result, when the network is trained, all the hidden units in a given row will have

learned the same weight pattern. Each row can be treated as a single unit replicated m times to examine m successive input slices as illustrated in Figure 4.11.

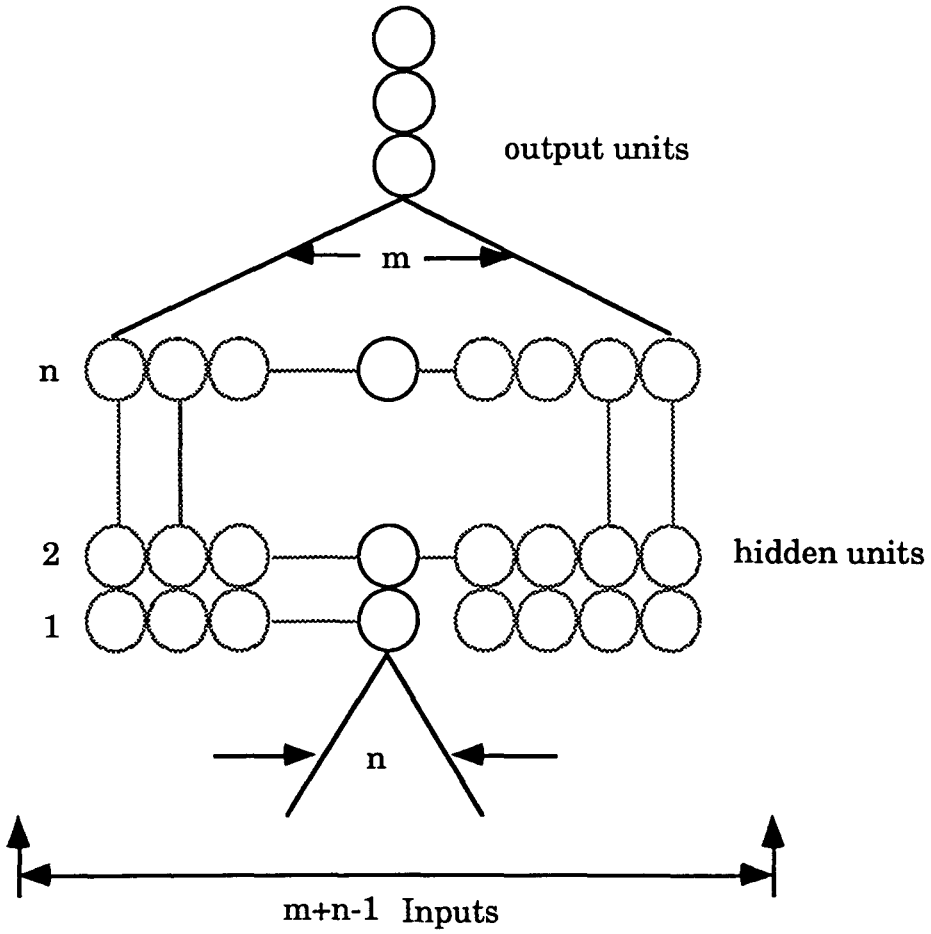

Figure 4.11 Equivalent TDNN representation [55]

The network effectively contains only n hidden units. Although the m copies of the hidden units posses identical weights, they can assume m different activation levels to represent the presence or absence of a feature in the m slices of the input. The same process is repeated for the output nodes. The modifications in the back-propagation algorithm for the TDNN is described next.

The error of a back-propagation network for a given case is a function of the differences between the network actual output o_j and the corresponding target values d_j, given as

$$E = \frac{1}{2} \sum_j (o_j - d_j)^2 \qquad (4.5)$$

For the MLP, the output values o_j of a network are the activation levels of its output units y_j. In case of the TDNN, there are two ways of combining the output responses. In the first method, each output value of the network is the average of the activations of several temporal replicas of an output unit, i.e.

$$o_j = \frac{1}{t} \sum_t y_{jt} \qquad (4.6)$$

where t is the number of time shifted copies of the output unit. The mean squared error in this case is

$$E = \frac{1}{2} \sum_j \left(\frac{1}{t} \sum_t y_{jt} - d_j \right)^2 \tag{4.7}$$

In the second method, each output value of the network is the sum of the squares of the activations of several temporal replicas of an output unit, i.e.

$$o_j = \sum_t y_{jt}^2 \tag{4.8}$$

The mean squared error is then

$$E = \frac{1}{2} \sum_j \left(\sum_t y_{jt}^2 - d_j \right)^2 \tag{4.9}$$

The weights are adapted to minimize the error in equation (4.7) using the back-propagation algorithm. The multiple shifted copies of the input signal used in this scheme forces the network to extract features in the data regardless of their temporal relationship.

CHAPTER 5

PREPROCESSING

The overall classification scheme used in this thesis is presented in Figure 5.1. Prior to the neural network classification, the signal is

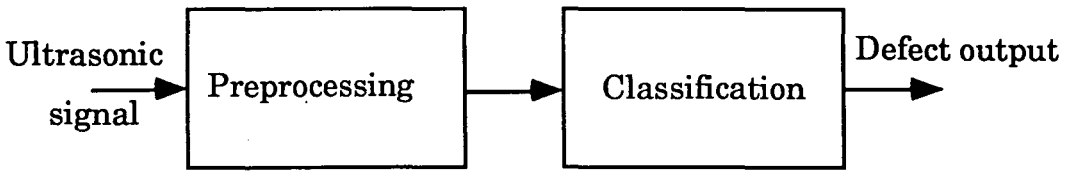

Figure 5.1 Overall classification scheme

first preprocessed. The preprocessing stage plays an important role in the characterization of the flaw. The input data typically consists of a mix of relevant and irrelevant information. Preprocessing serves to eliminate much of the irrelevant information and represents the relevant data in a compact and meaningful form. The compaction in turn results in the reduction of overall computational effort. This is important since neural networks, which are implemented on single processor systems, are extremely computationally intensive. Another important objective of preprocessing is to achieve invariance of classification performance under

translation of the input signal. Temporal variations in ultrasonic signals arise due to varying flaw depths and flaw locations. Neural networks are inherently sensitive to temporal shifts of the input signal. As a result, classification of ultrasonic signals using neural networks becomes sensitive to the location of the flaw in the material. By appropriately choosing the preprocessing technique, the features derived from the signal can be made insensitive to translations or rotations of the signal.

The choice of preprocessing techniques typically should meet the following criteria. Features should be selected in a manner that retains as much discriminatory information as possible. Second, the features should be rendered invariant under temporal shifts in the signal and be reasonably immune to effects of noise in the signal.

It is generally difficult to find a technique which meets all the above requirements at once. This chapter compares the effectiveness of numerous preprocessing techniques for characterizing ultrasonic signals. In addition to evaluating the performance of commonly used techniques such as

1. Spectral Coefficients.
2. Discrete Cosine Transform.
3. Cepstral Analysis.
4. Envelope Sampling.
5. Coarse Coding.
6. Autoregressive Modeling.
7. Principal Component Analysis.

the ultrasonic signal is also analyzed using the relatively new wavelet transform.

The preprocessing techniques are described next along with a discussion of their advantages and disadvantages. The theory and application of the wavelet function and wavelet transform is also developed later.

5.1 Spectral Coefficients

Spectral coefficients are the Fourier series expansion coefficients of a signal. The discrete Fourier transform (DFT) [56] of a sequence { x[n] }, n= 0,1,2,..N-1 is given as

$$X[k] = \sum_{n=0}^{N-1} x[n]\, e^{\frac{-j2\pi nk}{N}} \quad , k = 0, 1, \ldots N-1 \qquad n = 0,1, \ldots N-1 \tag{5.1}$$

where N is the number of samples in the input signal x[n].
Let y[n] be the time shifted version of x[n] expressed as

$$y[n] = x[n-n_o] \tag{5.2}$$

where n_o is the number of time units by which the signal is shifted.
Using the properties of Fourier Transform we have the relation

$$x[n-n_0] \quad <--> \quad X[k]\, e^{\frac{-j2\pi n_0 k}{N}} \tag{5.3}$$

$$\text{or} \quad Y[k] \quad = \quad X[k]\, e^{\frac{-j2\pi n_0 k}{N}} \tag{5.4}$$

The DFT of a sequence shifted in time is the same as the DFT of the unshifted sequence, times a phase factor. The magnitude of the X[k] and Y[k] are the same indicating that the magnitude of the spectral coefficients are independent of temporal shifts in the signal. This property makes it a suitable choice for characterizing ultrasonic signals.

The DFT of dimension N can be implemented using fast algorithms involving O(NlogN) operations [56]. Figure 5.2 shows the spectral coefficient sequence of an ultrasonic signal. As can be seen from the graph, most of the energy is concentrated in the first few coefficients. Hence, the signal can be expressed using a small number of DFT coefficients. To test the effectiveness of the technique, the neural network was first trained using the first 40 coefficients. The network was also trained using the first 30 coefficients, in an attempt to reduce the computational effort further.

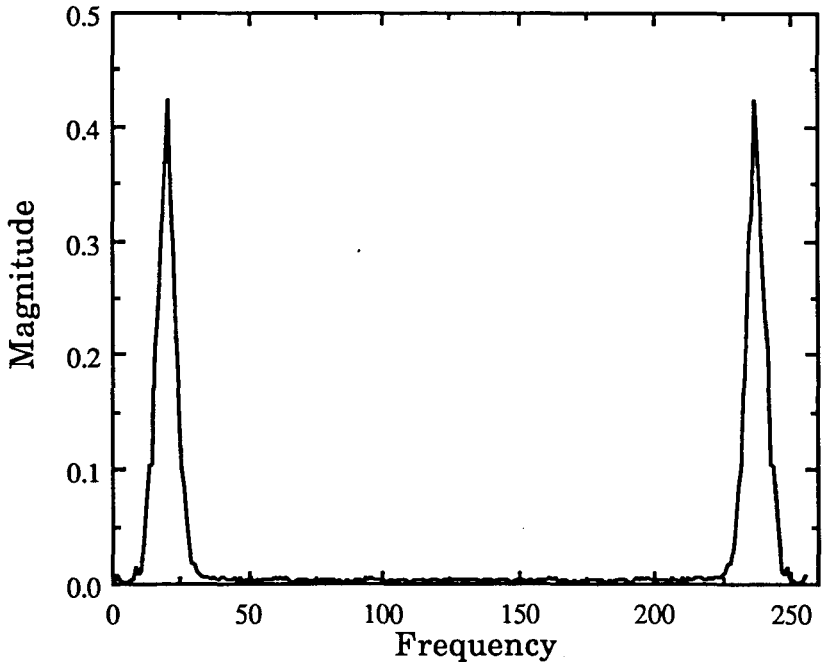

Figure 5.2 Spectral coefficients of ultrasonic signal

5.2 Discrete Cosine Transform

The discrete cosine transform (DCT) [57] of a sequence { x[n] } n=0,1,2,..N-1 is given as

$$X[k] = \alpha(k) \sum_{n=0}^{N-1} x[n] \cos\left[\frac{\pi(2n+1)k}{2N}\right] \quad \begin{matrix} k = 0, 1, \ldots . N-1 \\ n = 0, 1, \ldots . N-1 \end{matrix} \qquad (5.5)$$

where,

$$\alpha(0) = \sqrt{\frac{1}{N}} \quad \text{and} \quad \alpha(k) = \sqrt{\frac{2}{N}}, \quad k=1,2,...N-1$$

The DCT of a (N x 1) sequence { x(0), x(1), x(2), . . . x(N-1) } can be obtained from the DFT of a (2N x 1) symmetrically extended sequence of the form { x(N-1), x(N-2), ...x(1), x(0), x(0), x(1), ...x(N-2), x(N-1)}. The proof is presented in Appendix B.

The advantage of this method lies in the availability of many fast and efficient computational techniques for computing the real valued DCT coefficients. The DCT can be implemented in O(NlogN) operations using an N-point FFT algorithm. The DCT provides excellent energy compaction for highly correlated data. The correlation of a sequence { x[n] }, n=0,1,..N-1 can be expressed as

$$r(\tau) = \frac{1}{N} \sum_{n=0}^{N-1} x[n]\, x[n-\tau] \tag{5.6}$$

Figure 5.3 shows the correlation sequence of an ultrasonic signal. The corresponding DCT coefficients are plotted in Figure 5.4.

The disadvantage of this method is that the DCT coefficients of a signal are not time invariant. The neural network was trained using the first 30 as well as the first 40 coefficients as input, in an attempt to identify the discriminatory information present in the transformed signals.

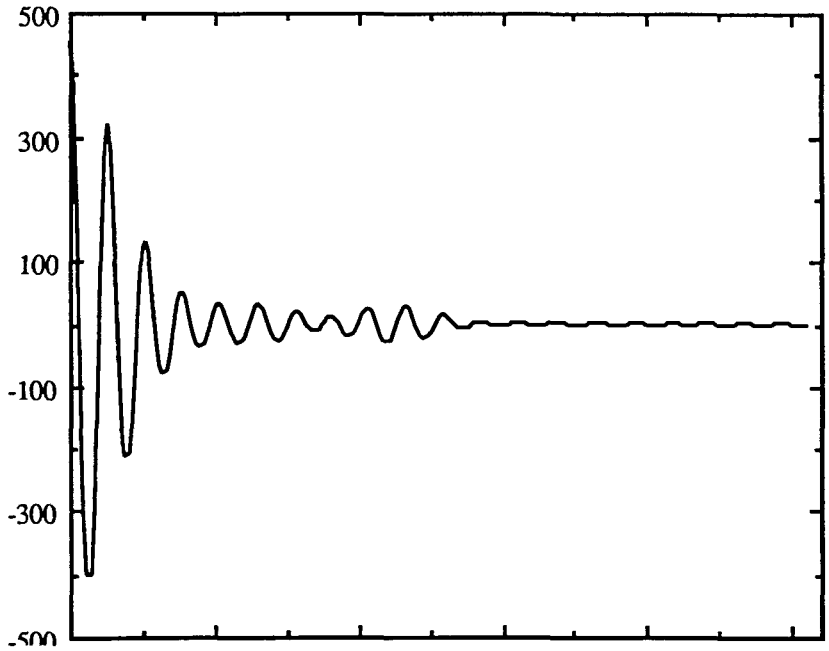

Figure 5.3 Correlation sequence of a typical ultrasonic signal

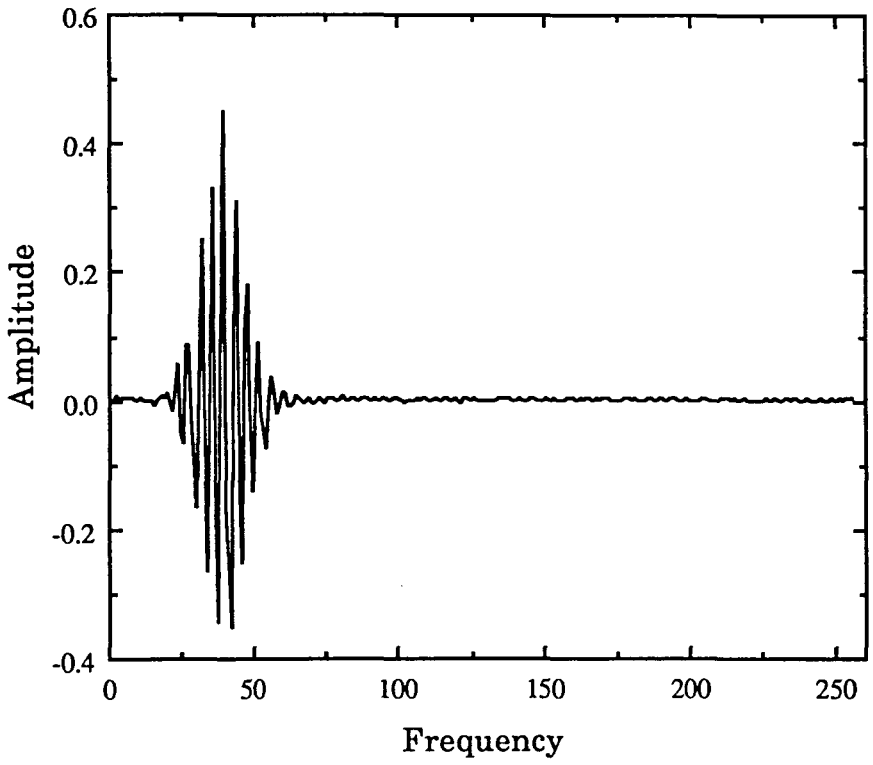

Figure 5.4 Discrete cosine transform coefficients of ultrasonic signal

5.3 Cepstral Analysis

In the pulse echo method of ultrasonic testing, the reflected signal, can be expressed as

$$y(t) = x(t) * h(t) \tag{5.7}$$

where x(t) represents the input signal. We also assume that the system is linear time-invariant with impulse response h(t), which models the propagation of sound through the medium in the direction along the beam. A more complete model for the received signal [58] would be

$$y(t) = u(t) * T_1(t) * P_1(t) * h_1(t) * P_2(t) * T_2(t) \tag{5.8}$$

where,

$u(t)$ = electrical impulse driving the transducer

$T_1(t)$ = forward transducer impulse response

$P_1(t)$ = forward propagation path impulse response

$h_1(t)$ = impulse response of scatter of interest (e.g. defect)

$P_2(t)$ = return propagation path impulse response

$T_2(t)$ = backward transducer impulse response

$$\text{If} \quad x(t) = u(t) * T_1(t) * P_1(t) \quad \text{and} \quad h(t) = h_1(t) * P_2(t) * T_2(t) \tag{5.9}$$

then,

$$y(t) = x(t) * h(t) \tag{5.10}$$

If h(t) is separated from the source x(t), one would have complete characterization of the material. Cepstral analysis is a deconvolution technique commonly used for estimating the impulse response.

The cepstrum [58,59] of a signal is the Fourier transform of the logarithm of the power spectrum. Taking the Fourier transform of equation (5.10) we get

$$Y(f) = X(f)\,H(f) \tag{5.11}$$

The power spectrum of the signal is represented as

$$|Y(f)|^2 = |X(f)|^2\,|H(f)|^2 \tag{5.12}$$

Taking the natural logarithm on both sides, we get

$$T(f) = 2\ln|Y(f)| = 2\ln|X(f)| + 2\ln|H(f)| \tag{5.13}$$

Thus, the multiplicative functions are transformed to additive ones and can be separated by appropriately filtering. The Fourier transform of equation (5.13) can be represented as

$$C(q) \leftrightarrow F\{T(f)\} \tag{5.14}$$

$$\therefore\ C(q) \quad <--> \quad 2\,F\ln|X(f)| + 2\,F\ln|H(f)| \tag{5.15}$$

where <--> denotes the Fourier Transform pair.

However, in the presence of noise $\eta(t)$ as shown in Figure 5.5, the reflected signal is represented as

$$y(t) = x(t) * h(t) + \eta(t) \tag{5.16}$$

The multiplicative properties of the spectrum do not hold any longer and as a result the performance of the cepstrum deteriorates.

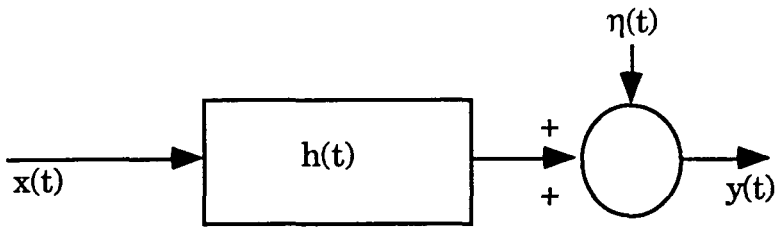

Figure 5.5 Output of linear system with additive noise

The cepstrum of the ultrasonic signal is shown in Figure 5.6. The first few cepstral coefficients were chosen as input to the classifier. The cepstral coefficients provide a time invariant representation.

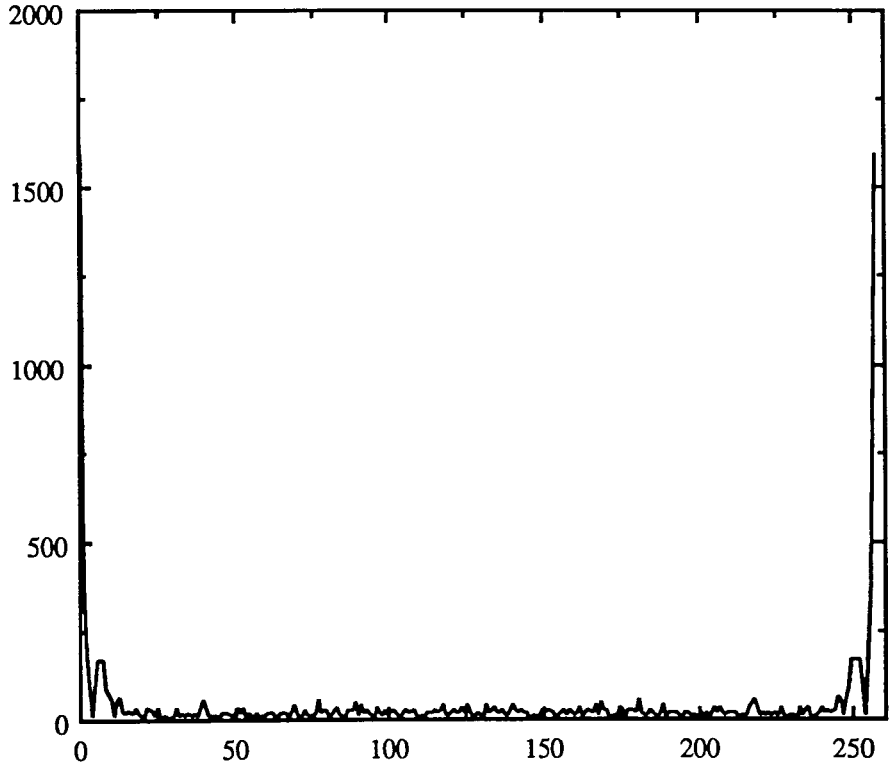

Figure 5.6 Cepstrum of ultrasonic signal

5.4 Envelope Sampling

This method is based on the use of the envelope of the time domain signal. The signal is sampled by extracting the peaks [11]. This operation reduces the dimensionality of the signal. In order to obtain time independent features the signal is centered. The algorithm for performing this operation is summarized below:

1. Rectify the signal and pick out a set of 50 maxima.
2. Center the 50 element array by placing the maximum peak in the middle of the array shifting the rest of the values accordingly.
3. Extend the input array by including the time intervals between the peaks.

Additional information about the envelope is retained in the form of time intervals between peaks. This information is appended to the 50 element array to form a 100 element input vector. The elements are normalized before being input to the neural network. Figure 5.7 shows a typical feature vector obtained using envelope samples of an ultrasonic signal.

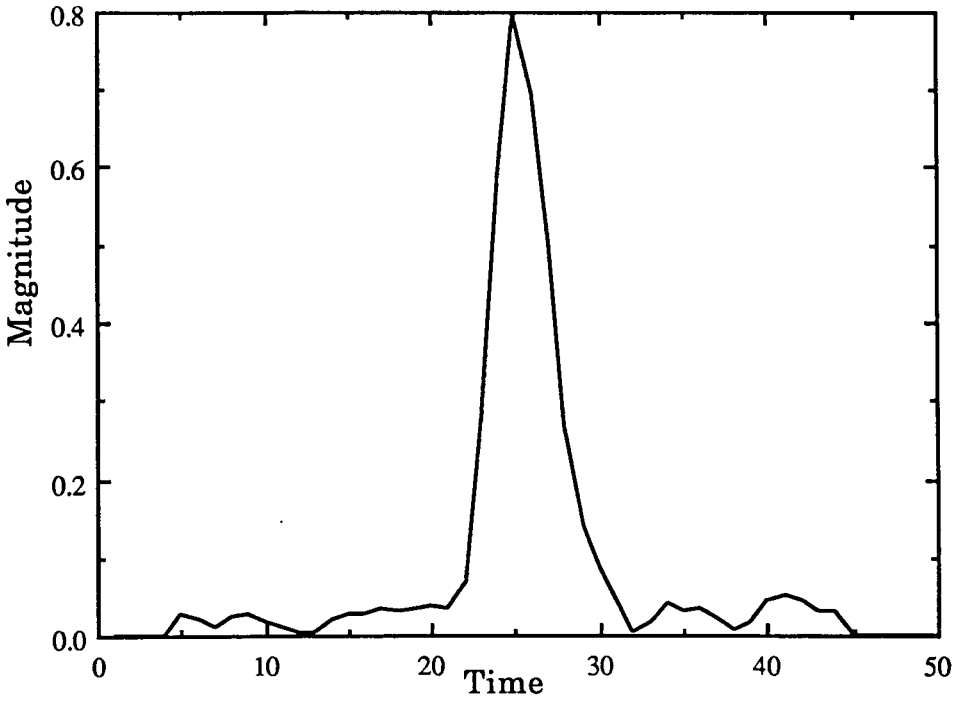

Figure 5.7 Envelope sampled ultrasonic signal

5.5 Coarse Coding

Another method of compressing information contained in the time domain signal is known as coarse coding. In this method the ultrasonic signal is divided into non-overlapping segments or bins as shown in Figure 5.8 and an input neuron is assigned to each zone or segment [39]. The segments chosen are fairly large to provide a relatively translation

invariant representation but small enough to accurately pinpoint location of the feature.

The ultrasonic signal was split into 8,16 and 32 non-overlapping segments and the integral of the signal spanning each segment was presented as input to the neuron. A typical time integrated ultrasonic signal using 16 bins is shown in Figure 5.9.

Coarse coding is effective when the features can be represented as an average of the features within each bin. Coarse coding provides translation invariance as well as added immunity to noise.

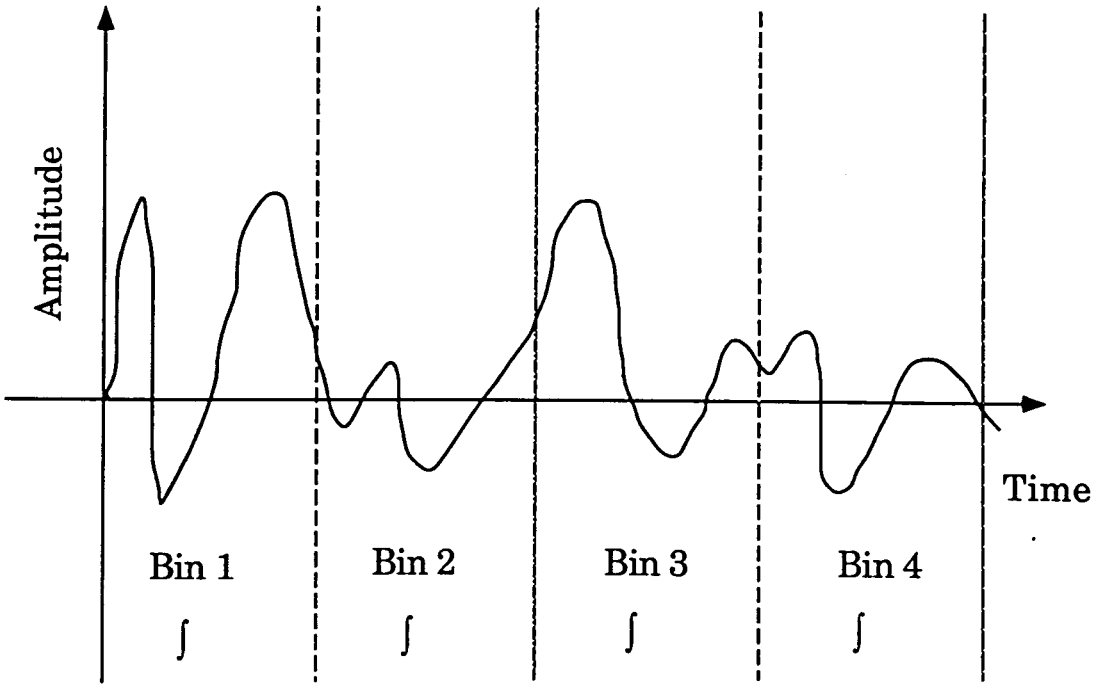

Figure 5.8 Coarse coding

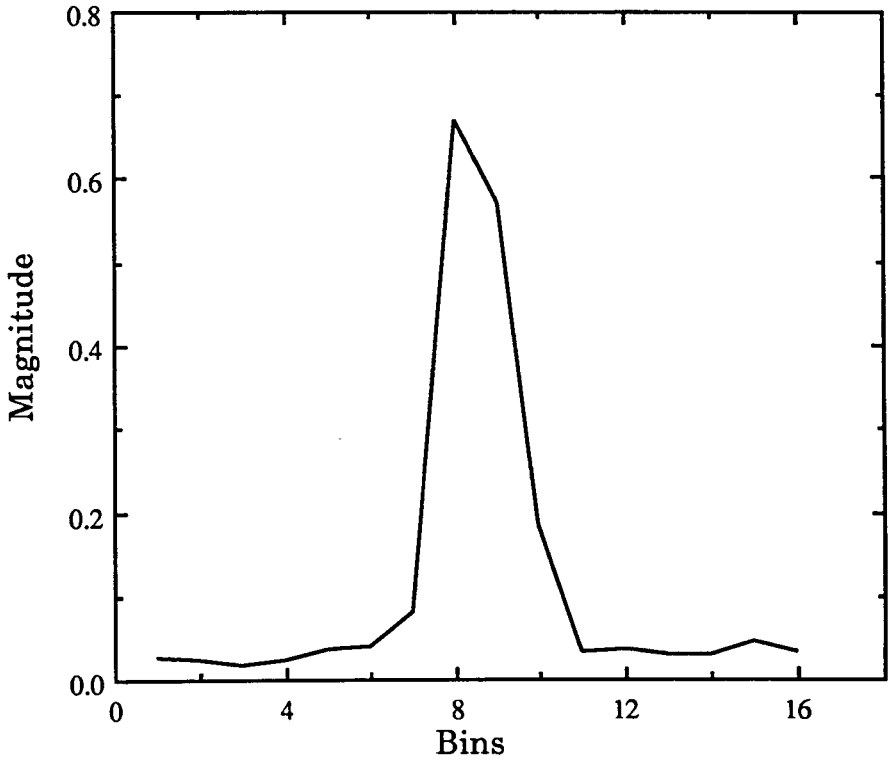

Figure 5.9 Coarse coded ultrasonic signal

5.6 Autoregressive Modeling

Autoregressive (AR) models treat the time domain signal between two consecutive backsurface reflectors as a stationary stochastic process. Irregular flaw shapes, grain boundaries and the inhomogenity of the materials serve as reflectors.

Let $\{ x_t \}$, t=1,2 . . . N be the sampled time series between two consective backsurface reflectors. Assuming a stationary stochastic process, we have

$$E\{ x_{p+n} , x_{k+n} \} = E\{ x_p , x_k \} \tag{5.17}$$

where,

p,k,n $\in$ N and E denotes the expectation operator

The time series is then represented by an AR model according to equation

$$x_t - \phi_1 x_{t-1} \ldots\ldots\ldots \phi_m x_{t-m} = a_t \tag{5.18}$$

where, the residual $\{ a_t \}$ is assumed to be normally distributed with zero mean and variance σ^2. The autoregressive coefficients of the model are given as $\{ \phi_i \}$, i=1,2 . . . m, where m represents the order of the model. Once the AR model is fitted, the input signal is condensed to a parameter vector $\underline{\theta}$ of dimension (m+1), where

$$\text{where } \underline{\theta}^T = (\underline{\phi}^T, \sigma_a^2) \tag{5.19}$$

and $\underline{\phi}^T = (\phi 1 \ldots\ldots \phi m)$ (5.20)

The AR model coefficients were computed using the Levinson-Durbin algorithm [58]. Although, this method provides data compression, the descriptors are not invariant under time shifts. The coefficients computed for various values of the model order m were presented as input to the neural network.

5.7 Principal Component Analysis

Another popularly used feature selection technique is the principal component analysis [60,61]. This method consists of finding an orthogonal transformation of the original variable to a new set of uncorrelated variables called principal components. The components are linear combinations of the original variables. The objective is to find, in the transformed feature space, fewer components to account for most of the variation in the original data set, effectively reducing the dimension of the signal.

Let $\{ x_t \}$, t=1,2, . . p represent the sampled time series. A linear orthogonal transformation of $\{ x_t \}$ with uncorrelated coefficients is of the form

$$\underline{z} = \phi^T \underline{x} \quad (5.21)$$

where $\underline{z} = (z_1, z_2 \ldots .z_m)^T$ with $m < p$, and ϕ is a mxp orthogonal matrix. Further,

$$E\{z_i z_j\} = 0 \quad i \neq j \qquad (5.22)$$
$$= 1 \quad i = j$$

The objective of this method is to determine the transformation matrix ϕ. The autocorrelation matrix of $\{x_t\}$, t=1,2,.. p is defined by the equation

$$R = \begin{bmatrix} r_0 & r_1 & \ldots . r_{p-1} \\ r_1 & r_0 & \ldots . r_{p-2} \\ \vdots & & \vdots \\ r_{p-1} & & r_0 \end{bmatrix} \qquad (5.23)$$

where $r_i = E\{x_t x_{t-i}\}$

It can be shown that the columns of the matrix ϕ can be formed by using the m eigenvectors, of the autocorrelation matrix, associated with the m largest eigenvalues λ_i of R.

Since the eigenvalues represent a measure of the interset variance, the eigenvectors represent the orthogonal directions, in the transformed space, that account for most of the variation in the original data set. The eigenvalues of the autocorrelation matrix are also known as the principal components of the signal. Singular value decomposition [62] routines can

be used is to obtain the λ_i values. Figure 5.10 shows the graph of the λ_i values for a typical ultrasonic signal.

It can be seen that the first few eigenvalues account for most of the variation in the original data set. The neural network was trained using varying number of eigenvalues as the input vector.

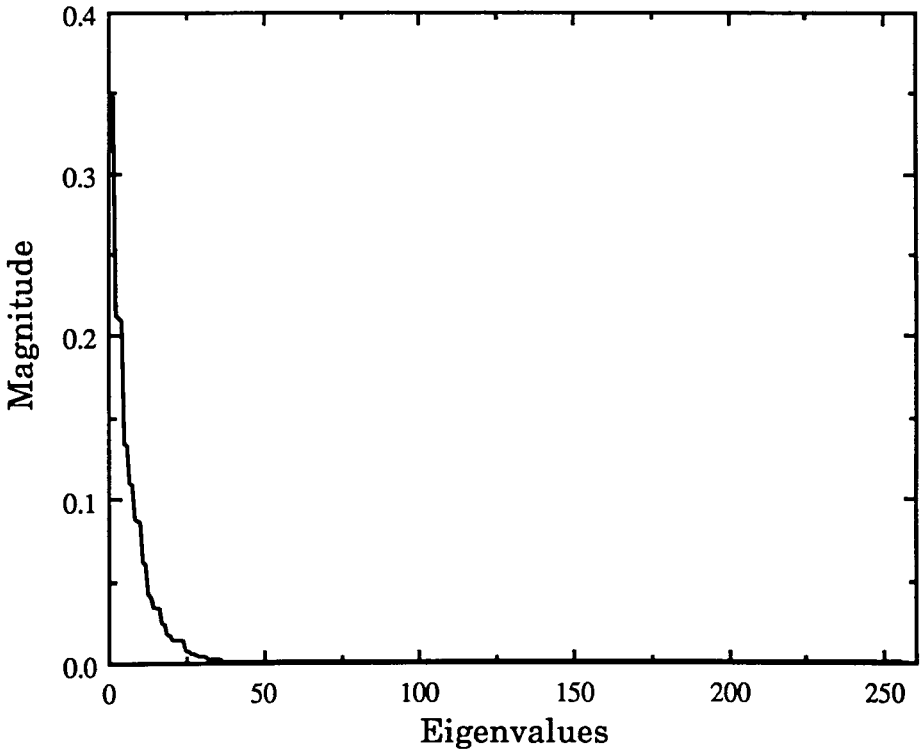

Figure 5.10 Eigen values of toeplitz (R) matrix for ultrasonic signal

5.8 Wavelet Transform

The aim of signal analysis is to extract relevant information from a signal by transforming it. For analysis of stationary signals, that is, signals whose properties do not evolve in time, the well known Fourier transform is used. The Fourier transform of a signal x(t) is expressed as

$$X(f) = \int_{-\infty}^{\infty} x(t)\, e^{-j2\pi f t} dt \qquad (5.24)$$

The analysis coefficients X(f) are computed as inner products of the signal with a sinusoidal basis function of infinite duration. As a result, any abrupt change in a non-stationary signal x(t) is spread over the entire frequency axis X(f). Therefore, the Fourier transform cannot be used for analyzing non-stationary signals.

The approach commonly used for analyzing non-stationary signals is known as Short Time Fourier Transform (STFT) [63]. STFT introduces time dependency in the Fourier analysis through a sliding window. The location of the sliding window adds a time dimension and one obtains a time-frequency analysis.

Consider a signal x(t) and assume it is stationary when seen through a window g(t) of finite support, centered at time location τ. The Fourier transform of windowed signal x(t) $g^*(t-\tau)$ yields the Short Time Fourier Transform (STFT) given as

$$S(\tau,f) = \int_{-\infty}^{\infty} x(t)\, g^{*}(t-\tau)\, e^{-j2\pi f t} dt \qquad (5.25)$$

which maps the signal onto a two dimensional function on the time-frequency plane (τ,f).

Once the window is chosen for the STFT, it is fixed over the time-frequency plane keeping the resolution same over the entire plane, as shown in Figure 5.11.

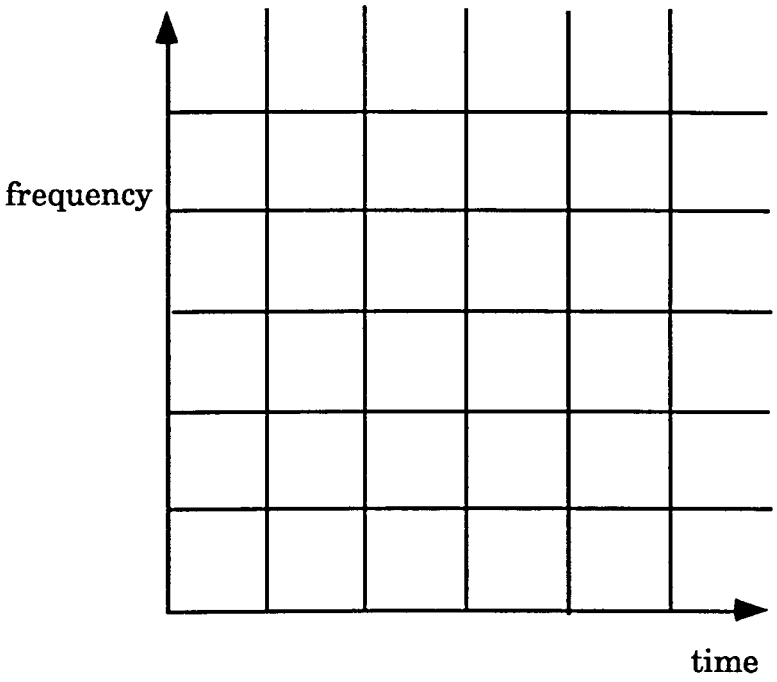

Figure 5.11 Time-frequency resolution with STFT [64]

With STFT each component within the signal can be analyzed with good time resolution or good frequency resolution but not both.To overcome the resolution limitation of the STFT, one must have a multi-resolution analysis providing both, good time and good frequency resolution [65]. This can be obtained using bandpass filters with constant relative bandwidth (i.e. $\Delta f/f$ = constant). Thus, instead of the filter being regularly spaced over the frequency axis as in the case of STFT, the filters are regularly spaced on the log frequency axis as shown in Figure 5.12.

Therefore, when the frequency resolution changes, so does the time resolution, satisfying the uncertainty principle where the product of time resolution and frequency resolution is constant.

The wavelet transform is a representation whose basis functions are well localized in time and frequency. The basis functions called the wavelets is defined as scaled (i.e. stretched or compressed) and translated version of the same prototype h(t) i.e.

$$h_{a,b} = \frac{1}{\sqrt{a}} h\left(\frac{t-b}{a}\right) \tag{5.26}$$

where a is the scale factor or the dilation parameter and b is the shift or the translation parameter. The constant $1/\sqrt{a}$ is used for energy normalization. As opposed to the STFT, the shape of the resolution cell varies with the scale parameter a. When a is small, resolution is coarse in the spatial domain and correspondingly fine in the frequency domain. When a is large, the resolution is fine is spatial domain and coarse in frequency domain as shown in Figure 5.13.

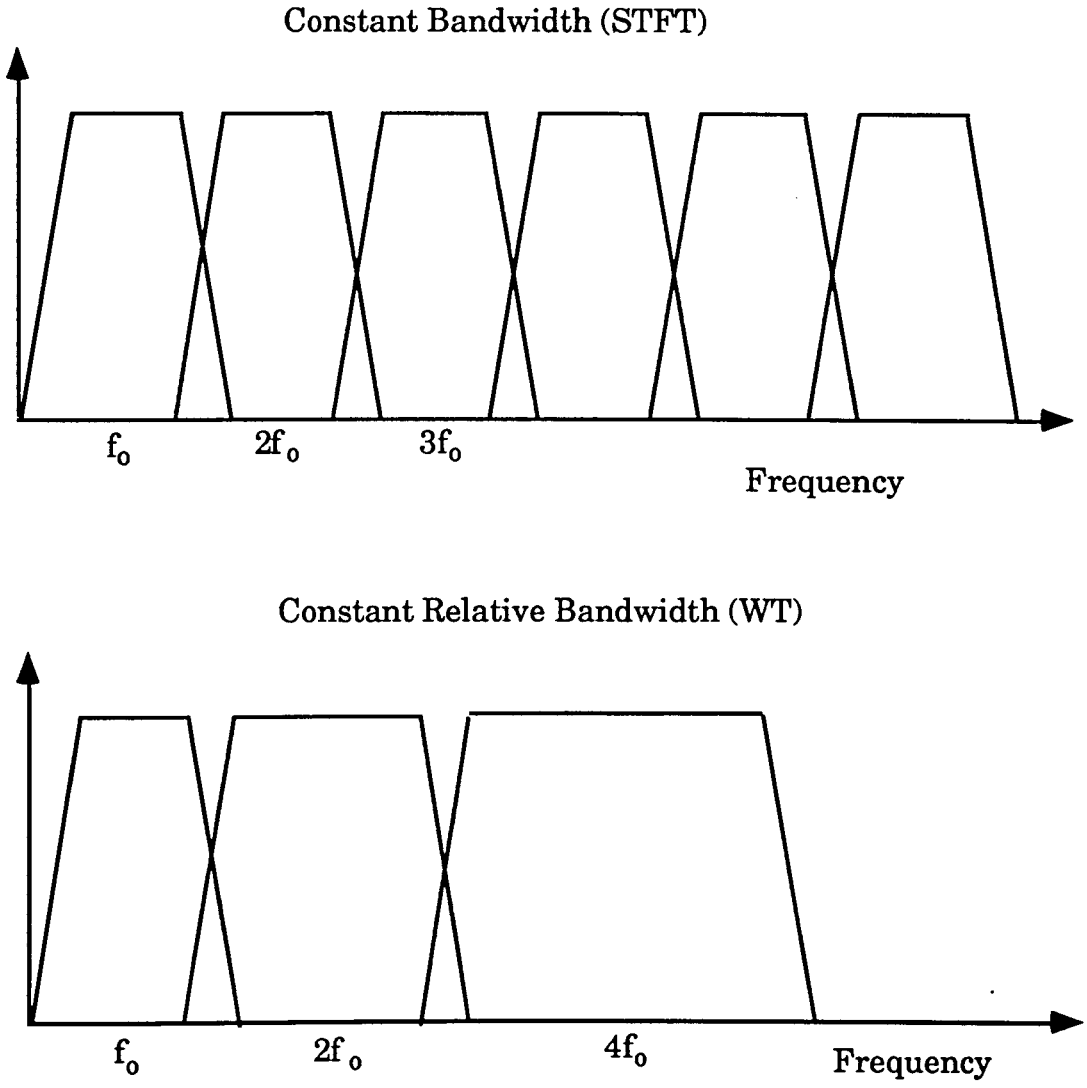

Figure 5.12 Bandpass filters for STFT and WT [64]

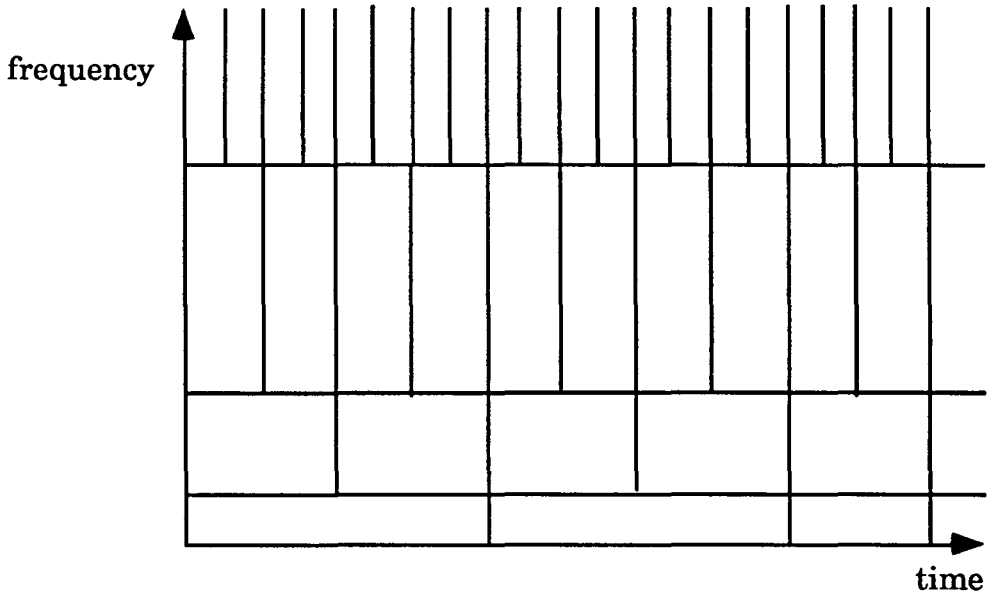

Figure 5.13 Time frequency resolution for WT [64]

The wavelet transform [66] of a signal s(t) can be represented as

$$W(a,b) = \frac{1}{\sqrt{a}} \int h^{*}\left(\frac{t-b}{a}\right) s(t)\, dt \qquad (5.27)$$

where,

a is the dilation parameter, > 0

b is the shift parameter

s(t) is the input signal

h(t) is the analyzing basis wavelet

W(a,b) is the transformed signal

In general, any signal can be represented as a combination of wavelets i.e. that the original waveform can be synthezied by adding elementary building blocks of constant shape but different widths and amplitude. The analysis is done using equation (5.27) and the synthesis process consists of summing up all the projections of the signal onto the wavelets as shown in equation (5.28).

$$x(t) = c\int\int_{a>0} W(a,b)\, h_{a,b}(t)\, \frac{dadb}{a^2} \qquad (5.28)$$

where c is a constant that depends only on h(t). The functions $h_{a,b}$ are in general not orthogonal, since they are defined for continously varying values of a and b. The reconstruction formula (5.28) is well defined if the wavelet satisfies certain conditions [64].

5.8.1 Constraints on the analyzing wavelet

The functional form of the analyzing wavelet must satisfy the following conditions.

1. h(t) is absolutely integrable and square integrable (e.g. finite energy)

$$\text{i.e.} \quad \int |h(t)|\, dt < \infty \quad \text{and} \quad \int |h(t)|^2 dt < \infty \qquad (5.29)$$

2. Also the low frequency behavior of h(t) must be such that

$$\int \frac{H(f)}{|f|} df \quad < \infty \tag{5.30}$$

where H(f) is the Fourier transform of h(t). The above condition implies that H(f) is a smooth function in the neighborhood of the frequency origin with H(0) = 0 which also implies that the true time domain function h(t) is zero mean.

5.8.2 Discrete Wavelet Transform

The wavelet transform can be discretized by sampling the scale parameter a and the shift parameter b. The scale parameter is varied logarithmically, so that

$$a = a_0^{\,m} \tag{5.31}$$

and the shift parameter b is sampled uniformly at a rate proportional to the scaling. This is accomplished by defining

$$b = n a_0^{\,m} b_0 \tag{5.32}$$

With these definations, the discrete wavelet transform can be represented using discrete valued parameters m and n as

$$W(m,n) = \frac{1}{\sqrt{a_0{}^m}} \sum h^*\left(\frac{t - n a_0{}^m b_0}{a_0{}^m} \right) s(t) \qquad (5.33)$$

$$W(m,n) = a_0^{-\frac{m}{2}} \sum h^*\left(a_0{}^{-m} t - n \right) s(t) \qquad (5.34)$$

The reconstruction equation is

$$x(t) = c \sum_m \sum_n W(m,n)\, h_{m,n}(t) \qquad (5.35)$$

where c is a constant that depends on h(t). For $a_0 = 2$ and $b_0 = 1$ the discrete wavelet transform [67] reduces to

$$W(m,n) = 2^{-\frac{m}{2}} \sum h^*\left(2^{-m} t - n \right) s(t) \qquad (5.36)$$

Figure 5.14 shows the sampling grid for the orthogonal wavelet implementation. This grid allows a precise reconstruction of the signal.

5.8.3 Wavelet Frames

The theory of wavelet frames [64,67] permits a balance between (i) redundancy and (ii) restrictions on the wavelet h(t) for accurate reconstruction. If the redundancy is large (high oversampling), then mild

restrictions have to be imposed on the basis function whereas if the redundancy is small, then the basis function must satisfy the required conditions.

The family of wavelet functions constitute a frame when the energy of the wavelet coefficients W(m,n) (sum of the square of the moduli) relative to that of the signal lies between two positive "frame bounds" A and B. i.e.

$$AE_x <= \sum_{m,n} |W(m,n)|^2 <= BE_x \qquad (5.37)$$

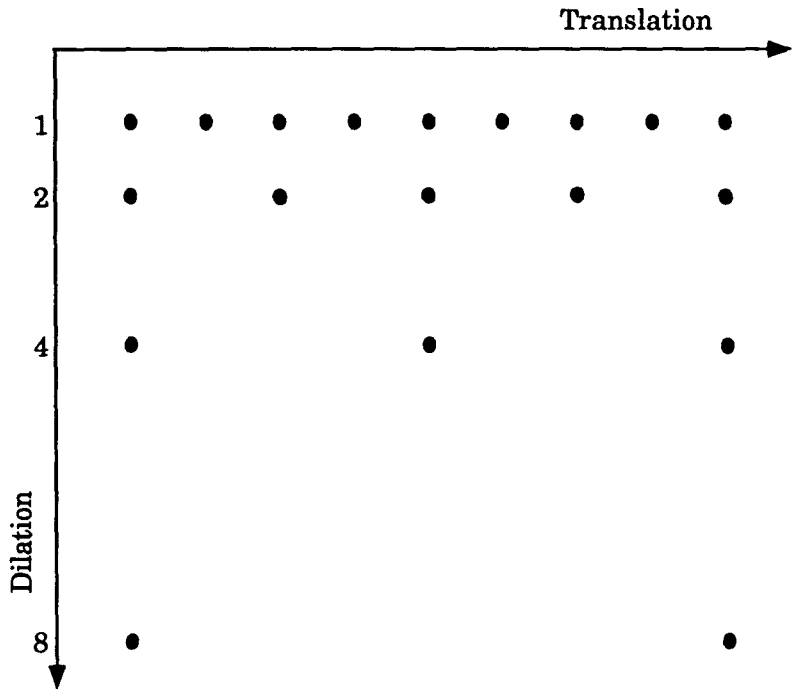

Figure 5.14 Sampling grid for discrete wavelet transform

where E_x is the energy of x(t). These frame bounds are computed from a_0, b_0 and h(t) [64,67]. The reconstruction equation can be written in terms of A and B as

$$x(t) = \frac{2}{A+B} \sum_m \sum_n W(m,n)\, h_{m,n}(t) \tag{5.38}$$

If A=B, the wavelet frame constitute a tight frame, in which case the wavelets behave exactly like an orthonormal basis [64,67].

5.8.5 Functional forms of the analyzing wavelet

Some of the wavelet functions used in these transforms are described below. The functional form of the Kronland-Martinent wavelet [68] is

$$h(t) = \exp\left(\frac{-t^2}{2} + j\omega t\right) \tag{5.39}$$

where, $\omega \approx 5.33$ for the wavelet to satisfy the admissibility condition.

Another function called the Mexican hat function [63] is defined by the equation

$$h(t) = (1 - t^2) \exp\left(\frac{-t^2}{2}\right) \tag{5.40}$$

The Figure 5.15 shows h(t) for few values of scaling and dilation.

The wavelet transform of ultrasonic signals were computed using the Mexican hat wavelet, for values of the scale parameter as 1,2,4,8,16 and 32. The transformed vectors for the different values of scaling are shown in figure 5.16-5.17. The transformed vectors were normalized and presented as input to the neural network.

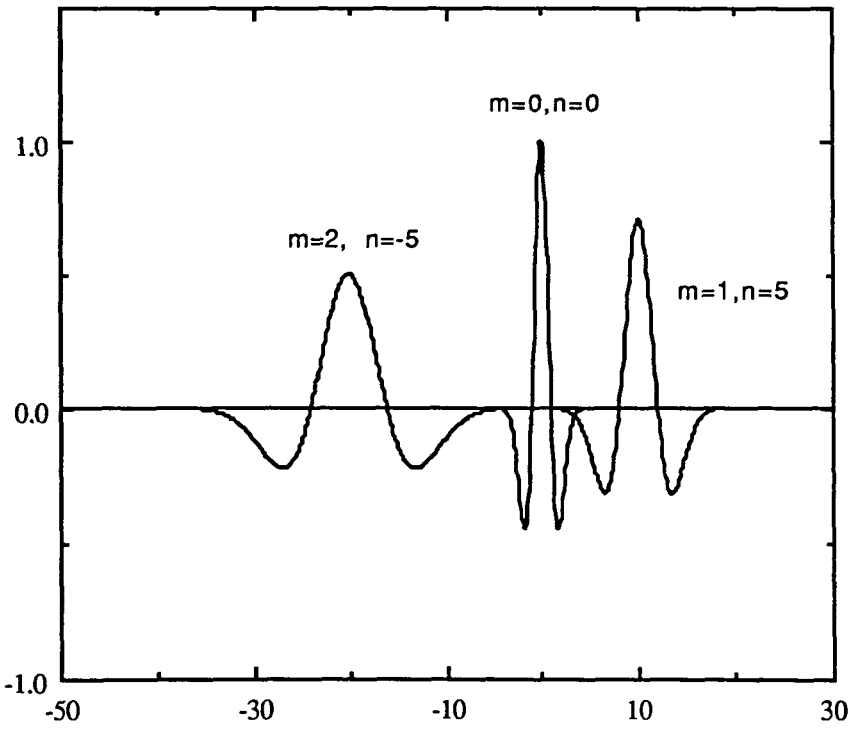

Figure 5.15 Mexican hat wavelet for m=0,1,2

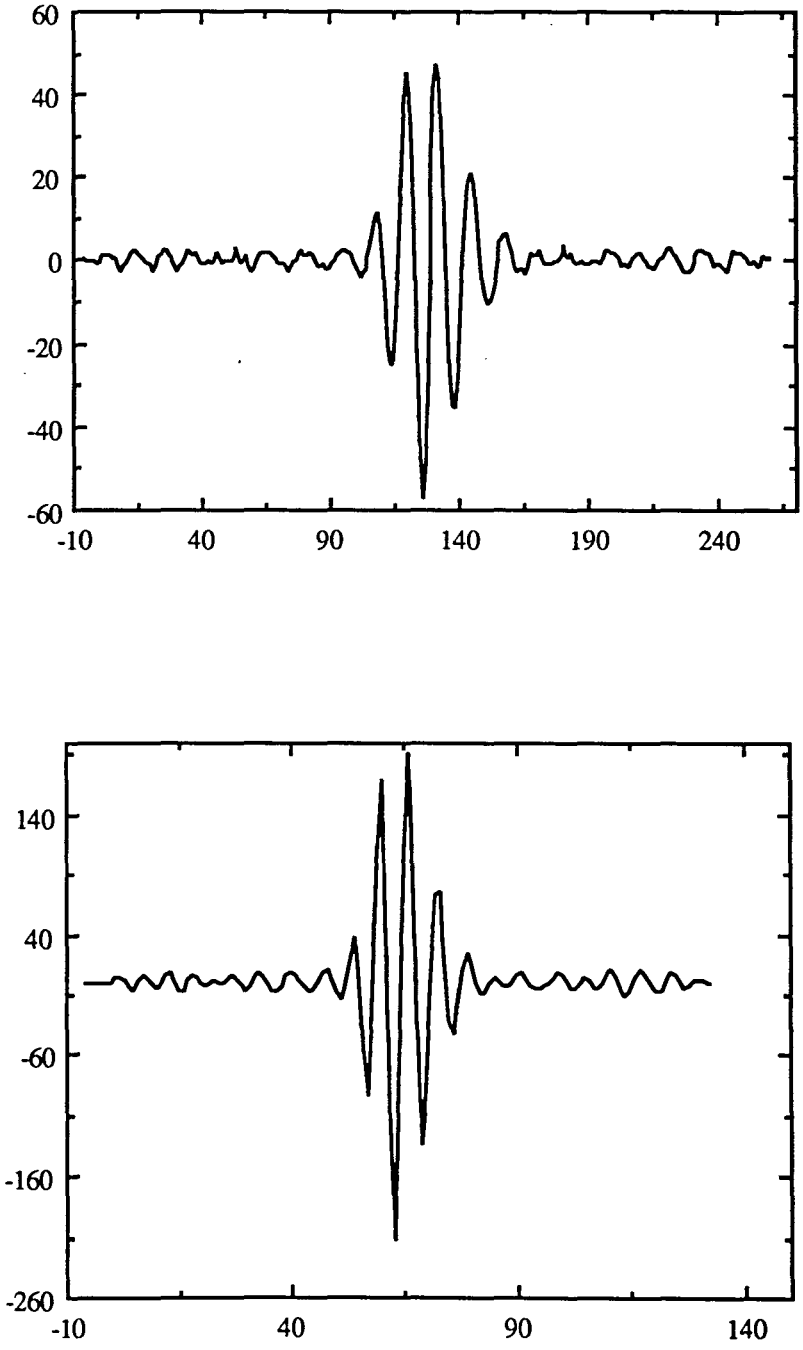

Figure 5.16 Wavelet transform of ultrasonic signal for m=0 and m=1

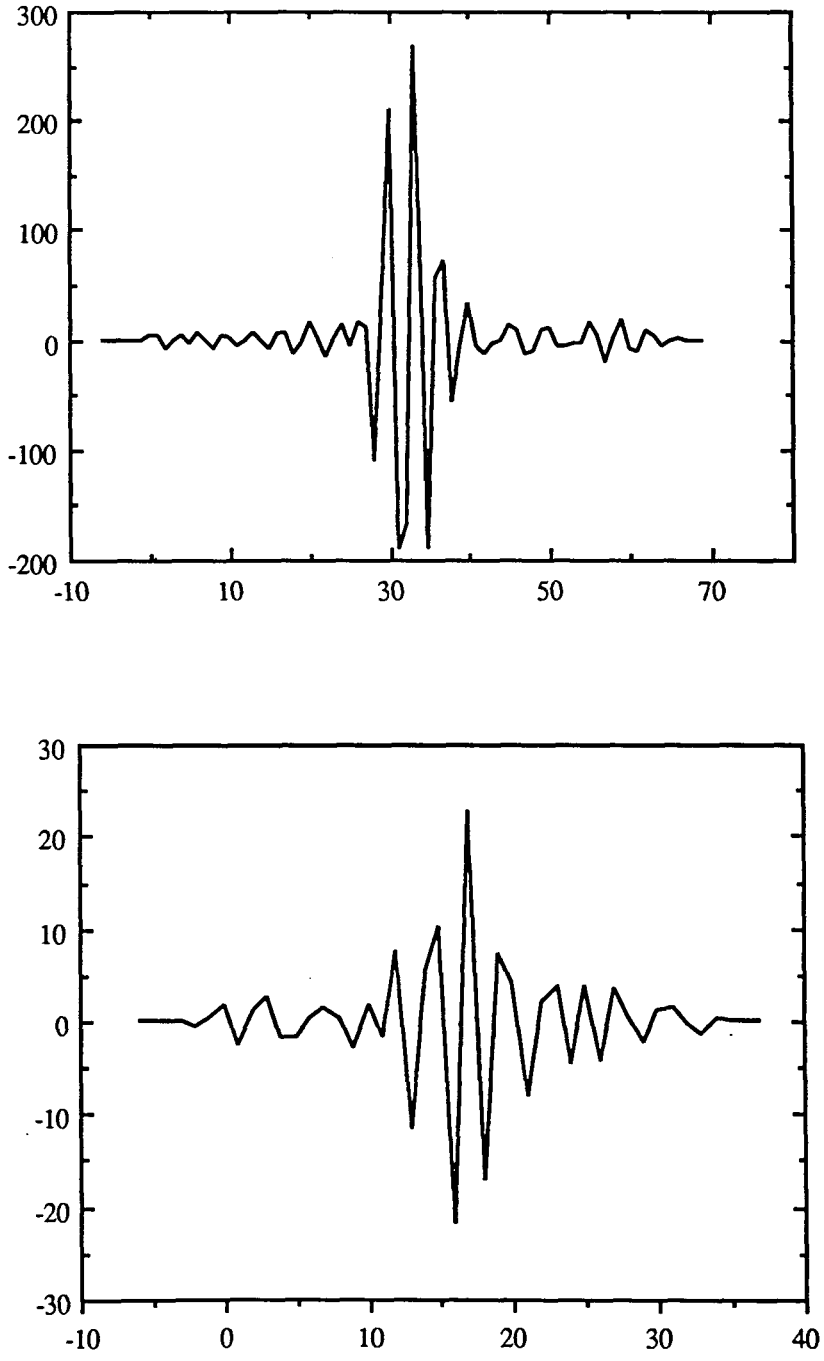

Figure 5.17 Wavelet transform of ultrasonic signal for m=2 and m=3

CHAPTER 6

RESULTS

6.1 Data set

A data set consisting of ultrasonic signal reflections belonging to three classes was analyzed. The first class of signals was from Intergranular Stress Corrosion Cracking (IGSCC) flaws in piping, whereas the last two class waveforms represent rootwelds and counterbores which are benign sources. A total of 909 signals were obtained, at a transducer frequency of 1.5 MHz. The signals were partitioned into three groups based on wall thickness of the piping inspected. Table 6.1 describes the three groups of signals.

Table 6.1 Description of the three groups of signals based on the range of wall thickness

Description	Wall thickness	Number of signals
Thinwalled	0.7 - 1.2	360
Midthickness	0.9 - 1.4	246
Thickwalled	1.2 - 1.5	303

The distribution of the signals in each class within each group is summarized in Table 6.2.

Table 6.2 Distribution of signals within each group

Group	Cracks	Couterbores	Rootwelds
Thinwalled	116	130	114
Midthickness	98	73	75
Thickwalled	120	99	84

Initially, the midthickness file was considered and the preprocessing techniques were implemented with the multi-layer perceptron for classification. Results were also obtained using the distance measures such as the Euclidean distance and the Similarity coefficient. The entire data set was later used for implementation of the multi-layer perceptron and the time delay neural network. This provided a better understanding of the generalization capability of neural networks in comparison to the other distance measures. The results also helped in the assessment of each technique.

Regardless of the network size 2/5 of the total signals were used for training, and the remaining 3/5 were used for testing. This provided an

effective means of comparison for different databases as well as network architectures. For each preprocessing technique employed, the number of nodes in the network was varied in an attempt to optimize the classification performance. Table 6.3 presents the results obtained with the multi-layer perceptron, using signals from the midthickness file.

The architecture of the network used is described in terms of the number of nodes in the input-hidden-output layers. Classification performance on both the training as well as the test data are shown.

The classification of signals in the midthickness file using conventional pattern recognition methods was then performed. The classification results with distance measures for different preprocessing techniques are presented in Table 6.4.

The algorithm was extended to the entire range of data including tubing of various wall thicknesses. Once again, the data was partitioned into a training set consisting of 2/5 of the signals. The results of classification using several preprocessing methods and the multi-layer perceptron as well as the TDNN are presented in Table 6.5. Results obtained using traditional classifiers are presented in Table 6.6 for comparison purposes.

Table 6.3 Classification results of signals in midthickness file using the multi-layer perceptron network

Preprocessing Technique	Architecture	Train	Test
DFT	30-15-3	95.96%	61.22%
	40-20-3	94.95%	61.90%
DCT	40-20-3	97.88%	66.67%
	30-15-3	92.93%	67.35%
Envelope Sampling	100-30-3	100.00%	82.31%
	100-40-3	100.00%	82.31%
Coarse Coding	16-10-3	98.99%	82.31%
	32-10-3	98.99%	78.91%
	8-4-3	96.57%	74.83%
Wavelet Transform	76-25-3	96.97%	70.75%
	44-20-3	96.97%	78.91%
	28-10-3	97.98%	86.39%
	20-10-3	95.96%	86.39%
	16-8-3	92.93%	88.44%
Principal Component Analysis	30-20-3	83.84%	65.99%
AR Modeling	10-5-3	61.18%	45.58%
Cepstral Analysis	50-25-3	62.63%	59.18%

Table 6.4 Classification results of signals in midthickness file using traditional pattern recognition techniques

Preprocessing	Number of Features	Euclidean Measure	Similarity Coefficient
DFT	40	59.86%	64.25%
	30	59.18%	64.25%
DCT	40	51.09%	50.64%
	30	60.36%	61.46%
Envelope Sampling	100	85.03%	86.39%
Wavelet Transform	16	62.58%	68.70%
	20	75.51%	78.91%
	28	74.82%	74.14%
	44	75.51%	70.06%
	76	70.74%	70.74%
Coarse Coding	8	71.48%	72.89%
	16	70.06%	70.06%
	32	70.74%	70.74%
Principal Component Analysis	30	55.78%	56.46%
	40	55.78%	56.46%
Cepstral Analysis	30	50.03%	51.79%
	40	50.34%	51.79%
AR Modeling	10	53.74%	53.96%

Table 6.5 Classification results of the entire data set using the MLP and TDNN

Preprocessing Technique	Architecture	Network	Test
DFT	30-15-3	MLP	79.27%
	40-20-3	MLP	76.70%
DCT	40-20-3	MLP	74.31%
		TDNN	76.15%
Envelope Sampling	100-30-3	MLP	78.90%
		TDNN	74.13%
	100-40-3	MLP	78.90%
		TDNN	73.76%
Coarse Coding	16-10-3	MLP	87.34%
		TDNN	84.95%
	32-10-3	MLP	86.42%
		TDNN	86.06%
	8-4-3	MLP	85.14%
		TDNN	81.83%
Wavelet Transform	76-25-3	MLP	86.24%
		TDNN	84.40%
	44-22-3	MLP	83.30%
		TDNN	77.98%
	28-20-3	MLP	82.94%
		TDNN	78.53%
	20-12-3	MLP	83.85%
		TDNN	77.80%
	16-8-3	MLP	84.77%
		TDNN	79.63%

Table 6.6 Results of the entire data set using traditional pattern classifiers

Preprocessing	Number of Features	Euclidean Measure	Similarity Coefficient
DFT	30	62.56%	62.20%
	40	63.12%	62.75%
DCT	30	60.36%	61.46%
	30	51.01%	50.64%
Envelope Sampling	100	73.21%	72.66%
Wavelet Transform	16	55.04%	57.98%
	20	67.88%	62.20%
	28	67.33%	63.85%
	44	73.94%	69.17%
	76	75.41%	70.45%
Coarse Coding	8	75.77%	73.21%
	16	74.86%	71.55%
	32	74.49%	70.27%

6.2 Postprocessing

In order to enhance the performance of the algorithm the misclassified signals were further analyzed. The analysis showed two types of classification errors which can be explained as follows.

The output assignments for the three different classes are given as:

Cracks	->	(001)
Counterbore	->	(010)
Rootwelds	->	(100)

The first type of misclassification involved incorrect classification where a signal due to a crack is incorrectly classified as (010), namely a counterbore. In the second type of misclassification the network gives an invalid output such as (011) or (000). These signals are labelled as "ambiguous" and are resolved using a postprocessing method. The addition of a postprocessor resulted in significant improvement in performance.

Two different types of postprocessing were considered. The first method is based on the node which has the highest output level. This can be best understood with the help of an example. A network output of (0,0.2,0) is treated by the network as class (000) which indicates ambiguous classification. The postprocessing assigns the signal to the class based on the node which has the highest level of output namely (010). In the second

method a simple mapping function was derived such that the overall classification error was minimized. The following mapping was used.

Invalid output		Class
(000)	->	(001)
(011)	->	(010)
(101)	->	(100)
(110)	->	(100)

For example, the output of (000) is treated as a crack belonging to class (001) and so on. The mapping scheme was derived on the basis of the results obtained during the training phase. The results obtained using postprocessing are shown in Table 6.7. From Table 6.7 it can also be observed that the classification performance using the TDNN is slightly lower than that obtained using the MLP for the same architecture. However, the TDNN tends to have a fewer number of incorrect classifications. Table 6.8 shows the number of classification errors using the MLP and the TDNN.

Table 6.7 Classification results with postprocessing

Preprocessing Technique	Network	Test	Post processing	
			Mapping	Max. Node
DFT	MLP	79.27%	84.15%	83.10%
DCT	MLP	74.31%	80.50%	81.65%
	TDNN	76.15%	82.10%	83.60%
Envelope Sampling	MLP	78.90%	82.56%	82.20%
	TDNN	74.13%	82.20%	83.85%
Coarse Coding	MLP	87.34%	89.17%	89.70%
	TDNN	84.95%	89.49%	88.60%
Wavelet Transform	MLP	86.24%	89.17%	88.90%
	TDNN	84.40%	88.25%	90.27%

Table 6.8 Analysis of misclassifications with the MLP and the TDNN

	Envelope Sampling	Coarse Coding	Wavelet Transform	DCT
MLP	14.10%	7.20%	7.90%	11.94%
TDNN	9.10%	6.20%	5.50%	11.00%

CHAPTER 7

SUMMARY, CONCLUSIONS AND FUTURE WORK

Ultrasonic NDT is used extensively for detecting intergranular stress corrosion cracking (IGSCC) in nuclear power plant tubing. Detection of IGSCC is made difficult due to the close resemblance of IGSCC signals to signals form nearby weld joint physical features, such as rootwelds and counterbores. In addition, the presence of temporal shifts in the reflected ultrasonic signal due to varying flaw locations and varying flaw depths, makes classification of ultrasonic NDT signals a difficult task. This thesis evaluates the application of various signal processing techniques for ultrasonic flaw characterization.

The overall defect characterization scheme consists of three major modules. The first step in the classification process is preprocessing. The preprocessing stage renders the classification result relatively immune to effects of temporal variations in the signal. The preprocessing also compresses the data which in turn reduces the computational effort. Several preprocessing methods were evaluated in an attempt to find optimal features for characterizing ultrasonic signals. In addition to evaluating the performance of commonly used techniques such as spectral coefficients, discrete cosine transform, autoregressive modeling, principal component analysis and cepstral analysis, techniques such as coarse coding, envelope sampling and the relatively new wavelet transform were investigated. Most

of the above preprocessing techniques provide both data compression and time invariance.

The wavelet transform represents the signal using an orthogonal set of basis functions, well localized in time and frequency. These basis functions called wavelets are scaled and translated versions of a prototype wavelet. This method provides multi-resolution analysis by changing the scale parameter.

The next step in the classification process is the classifier. This thesis uses the multi-layer perceptron (MLP) for the characterization of ultrasonic signals obtained during inspection of nuclear power plant tubing. A major advantage of the multi-layer perceptron is its ability to generate highly non-linear decision surfaces in the multi-dimensional feature space. In addition, these networks do not require apriori statistical information. Also, once the network is trained, classification of unknown signals can be implemented in real time. Alternate architectures, such as the time delay neural network (TDNN) was also investigated. The TDNN offers the advantage of invariance under temporal shifts in the signal.

The final step in the classification process is postprocessing, which is included to help reduce the error caused by ambiguous classification.

Classification results were obtained using features extracted with the above preprocessing schemes in conjunction with the MLP and the TDNN. The classification performance is seen to be sensitive to the choice of network parameters and most importantly to the choice of features. Features computed using coarse coding, envelope sampling and the wavelet transform

demonstrated good performance. The TDNN seemed to have lower percentage of misclassifications in comparison to the MLP.

The wavelet transform analysis studied in this thesis shows considerable promise for representing and classifying ultrasonic NDT signals. However, there are several issues that require further study. Firstly, a major drawback of the back-propagation algorithm is convergence to local minima which results in suboptimal estimates of the decision boundary used in the classification. Alternate algorithms for determining globally optimal solutions will enhance classification performance. In addition, a systematic method for arriving at the optimal network architecture is needed.

In conclusion, artificial neural networks combined with appropriate preprocessing provide an exciting prospect for classifying ultrasonic signals in real time. The classification performance obtained using the various preprocessing techniques indicates the need for good preprocessing for successful flaw characterization.

REFERENCES

[1] Udpa, L., and Udpa, S.S. "Application of Neural Networks to Nondestructive Evaluation." Proceedings of the First IEE Conference on Artificial Neural Networks, London, England, October, 1989.

[2] Shankar, R., Williams, R., and Avioli, M.J. "An expert system for Power Plant NDE." A Review of Progress in Quantitative NDE edited by D. O. Thompson and D. Chimenti, Vol. 8A, New York: Plenum Press, 1989, pp. 665.

[3] Udpa, L., Lord, W., and Udpa, S.S. "Multifrequency Eddy Current Data." A Review of Progress in Quantitative NDE edited by D. O. Thompson and D. Chimenti, Vol. 8A, New York: Plenum Press, 1989, pp. 329.

[4] Krautkramer, J., and Krautkramer, H. Ultrasonic Testing of Materials. New York: Springer-Verlag, 1977.

[5] Szilard, J. Ultrasonic Testing. New York: John Wiley and Sons, 1982.

[6] Ludwig, R. "The Finite Element Modeling of Ultrasonic NDT Phenomena." Ph.D. dissertation, Colorado State University, Ft. Collins, Colorado, 1986.

[7] Thompson, R. B., and Thompson, D. O. "Ultrasonics in Nondestructive Evaluation." Proceedings of the IEEE, December, 1985, pp. 1716.

[8] Graff, K.F. Wave Motion in Elastic Solids. Oxford: Clarendon Press, 1975.

[9] McMaster, R.C. Nondestructive Testing Handbook. Columbus: The American Society for Nondestructive Testing, Inc., 1959.

[10] Carlin, B. Ultrasonics. New York: McGraw-Hill Book Company, Inc., 1960.

[11] Berry, D. "The Application of Neural Networks to Ultrasonic Signals." M.S. Thesis, Colorado State University, Ft. Collins, Colorado, 1989.

[12] Mix, P.E. Introduction to Nondestructive Testing, A Training Guide, New York: John Wiley and Sons, 1987.

[13] Halmshaw, R. Nondestructive Testing, London: Edward Arnold, 1987.

[14] Houghton, J., and Shen, P. "Ultrasonic reflector classification with Autoregressive Models." Research in Nondestructive Evaluation, Vol. 1, No. 4, 1990, pp. 235.

[15] The Institution of Metallurgists. Ultrasonic Non-Destructive Testing. London.

[16] Udpa, S.S., and Singh, G.P. "The role of digital signal processing in NDT." NDT International, Vol. 19, No. 3, June, 1986, pp. 125.

[17] Lewis. W., Sproat, W., Dodd, B., and Hamilton, J. Reliability of Nondestructive Inspections. Rep. AS-ALC/MME 76-6-38-1, San Antonio Air Logistics Center, Kelley Air Force Base, Texas, 1978.

[18] Behrauseh, M., Karimi, S., and Ford, M. "Human Factor Affecting the Performance of Inspection Personnel in Nuclear Power Plants." A Review of Progress in Quantitative NDE edited by D. O. Thompson and D. Chimenti, Vol. 8B, New York: Plenum Press, 1989, pp. 2235.

[19] Taylor, T., Spanner, J., Heasler, P., Doctor, S., and Deffenbaugh, J. "An Evaluation of Human Reliability in Ultrasonic In Service Inspection for Intergranular Stress Corrosion Cracks Through Round Robin Testing." Materials Evaluation, March, 1989, pp. 338.

[20] Saniie, J., Wang, T., Bilgutay, N.M. "Optimal ultrasonic flaw detection using a frequency diversity technique." A Review of Progress in Quantitative NDE edited by D. O. Thompson and D. Chimenti, Vol. 8A, New York: Plenum Press, 1989, pp. 751.

[21] Burch. S., and Bealing, N. "A Physical approach to the automated Ultrasonic Characterization of Burried Weld Defects in Ferrite Steel." NDT International, June,1986, pp. 145.

[22] Doctor. S.R., Hall, T.E., and Reid, L.D. "SAFT- the evolution of a signal processing technology for ultrasonic testing." NDT International, June, 1986, pp. 163.

[23] Sharpe, R.S. Research Techniques in Nondestructive Testing, Vol. VI, Orlando, Florida: Academic Press, 1987.

[24] Ghorayeb, S.R., Hughes, M.S., Holger, M.S., and Zachary, L.W. "A Preliminary Application of SAFT on Composites." A Review of Progress in Quantitative NDE edited by D. O. Thompson and D. Chimenti, Vol. 10A, New York: Plenum Press, 1991, pp. 1027.

[25] Brown, R.L. Investigating the Computer Analysis of Eddy Current NDT Data. HEDL-SA-1721, Hanford Engineering Development Laboratory, Richland, Washington, February, 1979.

[26] Mucciardi, A.N. "Elements of Learning Control Systems with Applications to Industrial Processes." Proceedings of the IEEE Conference on Decision and Control, New Orleans, 1972.

[27] Udpa, S.S. "Parametric Signal Processing for Eddy Currrent NDT." Ph.D. dissertation, Colorado State University, Ft. Collins, Colorado, 1983.

[28] Doctor, P.G. et al. "Pattern Recognition Methods for Classifying and Sizing Flaws Using Eddy-Current Data." Eddy Current Characteristics of Materials and Structures, ASTM STP 722, G. Birnbaum and G. Free, Editors, American Society for Testing and Materials, 1981, pp. 461.

[29] Rose, J.L., Jeong, Y.H., Alloway, E., and Copper, C.T. "A Methodology for Reflector Classification Analysis in Complex Welded Structures." Materials Evaluation, Vol. 42, No. 1, January, 1984, pp. 98.

[30] Saniie, J., Wang, T., Jin, X., and Bilgutay, N.M. "Application of Linear Prediction Analysis in Ultrasonic Grain Signal Characterization." A Review of Progress in Quantitative NDE edited by D. O. Thompson and D. Chimenti, Vol. 8A, New York: Plenum Press, 1989, pp. 681.

[31] Shirvaiker, M., and Musari, M. "A neural network classifier for character recognition." INNS Abstracts, Neural Network Supplement, January, 1988, pp. 524.

[32] Guez, A., Elibert, J. and Kam, M. "Neural Network architecture for control." IEEE Control Systems Magazine, April, 1988, pp. 22.

[33] Martinetz, T. M., Ritter, H.J., and Schutten, K.J. "Three Dimensional Neural Net for learning Visuomotor Coordination of a Robot Arm." IEEE Transactions on Neural Networks, March ,1990, pp. 131.

[34] Burr,D. "Speech Recognition experiments with perceptrons." Proceedings of the 1987 IEEE Conf. on Neural Info. Proc. Sys. - Natural and Synthetic, New York: American Institute of Physics, 1988, pp. 144.

[35] Dietz, W., Kiech, E., and Ali, M. "Pattern based fault-diagnosis using neural networks." First International Conference on Industrial and

Engineering Applications of AI and Expert Systems, University of Tennessee Space Institute, Chattanooga, Tenessee, 1988, pp. 13.

[36] Kandel, E.R., and Schwartz, H.J. Principles of Neural Science, Amsterdam: Elsevier Science Publishing Co., 1985, pp. 13.

[37] Simpson, P.K. Artificial Neural Systems, New York: Pergamon Press, 1990.

[38] Lippman, R. "An Introduction to Computing with neural nets." IEEE ASSP Magazine, April,1987, pp. 4.

[39] Rummelhart, D., and McClelland, J. Parallel Distributed Processing, Exploration in the Microstructure of Cognition, London: MIT Press, 1988.

[40] Castelez, P. "Neural Networks in defense applications." Proceedings of IEEE International Conference on Neural Networks, Vol. II, San Diego, 1988, pp. 473.

[41] Bourland, H., and Wellekens, C. "Multi-layer perceptrons and automatic speech recognition." Proceedings of the IEEE First International Conference on Neural Networks, Vol. IV, San Diego, 1987, pp. 407.

[42] Sobajic, S., Lu, J-J., and Pao, Y-H. "Intelligent control on the intelledex 605T robot manipulator." Proceedings on the IEEE International Conference on Neural Networks , Vol. II, San Diego, 1988, pp. 663.

[43] Dayhoff, R., and Dayhoff, J. "Segmentation of true color microscopic images using backpropagation neural network." INNS Abstracts, Neural Network Supplement, January, 1988, pp. 169.

[44] Bounds. D., Lloyd, P., Mathew, B., and Waddell, G. "A multilayer perceptron network for the diagnosis of low back-pain." Proceedings of

the IEEE International Conference on Neural Networks, Vol. II, San Diego, 1988, pp. 481.

[45] Gorman, P., and Sejnowski, T. "Learned classification of sonar targets using a massively parallel network." IEEE Transactions on Acoustics Speech Signal Processing, Vol. 36, pp. 1135.

[46] Plaut, D.C., Nowlan, S.J., and Hinton, G.E. Experiments on learning by Back-Propagation. Carnegie-Mellon University, Pittsburgh, PA, Report CMU-CS-86-126, 1986.

[47] Chow, J. "Neural Networks using Homotopy Continuation Methods." M.S. Thesis, Iowa State University, Ames, Iowa, 1991.

[48] Ash, T. Dynamic node creation in backpropagation networks. University of California at San Diego, Institute of Cognitive Science Technical Report 8901, 1988.

[49] Pemberton, J., and Vidal, J. " When is the generalized delta rule a learning rule ?" Proceedings of the IEEE International Conference on Neural Networks: Vol. I, San Diego, 1988, pp. 309.

[50] Canillon, J., Andeniol, B., and Markade, E. "Constrained back - propagation." INNS Abstracts, Neural Networks Supplement, January, 1988, pp. 539.

[51] Werbos, P. "Beyond Regresion: New tools for prediction and analysis in behavioral sciences." Ph.D. Dissertation, Harvard University, 1974.

[52] Jordan, M. Serial order: A parallel distributed processing approach, University of California at San Diego, Institute for Cognitive Science Technical Report 8604, 1986.

[53] Klassen, M., Pao, Y-H., and Chen, V. "Characteristics of the functional link net: A higher order delta rule net." Proceedings of the IEEE International Conference on Neural Networks, Vol. I, San Diego, 1988, pp. 507.

[54] Waibel, A., Hanazawa, T., Hinton, G., Shikano, K., and Lang, K. "Phoneme Recognition using Time-Delay Neural Networks." IEEE Transactions on Acoustics, Speech and Signal Processing, March, 1987, pp. 328.

[55] Lang. K., and Hinton, G. A Time-Delay Neural Network Architecture for Speech Recognition. Carnegie-Mellon University, Pittsburg, PA, Tech. Rep. CMU-CS-88-152, December, 1988.

[56] Oppenheim, A.V., and Schafer, R.V. Discrete Time Signal Processing, Englewood Cliffs, New Jersey: Prentice Hall, 1986.

[57] Jain, A.K. Fundamentals of Digital Image Processing, Englewood Cliffs, New Jersey: Prentice Hall, 1989.

[58] Parsons, T. Voice and Speech Processing, New York: Mc-Graw Hill, 1986.

[59] Chen, C.H. Signal Processing Handbook, New York: Marcel Dekker, Inc., 1988.

[60] Lohnes, C. Multivariate Data Analysis, Malabar, Florida: Robert E. Krieger Publishing Company, 1985.

[61] Chatfield, C., and Collins, A.J. Introduction to Multivariate Analysis, New York: Chapman and Hall, 1980.

[62] Press, W.H., Flannery, B.P., Teukolsky, S.A., Vetterling, W.T. Numerical Recipes in C. New York: Cambridge University Press, 1990.

[63] Daubechies, I. "The Wavelet Transform, Time-Frequency Localization and Signal Analysis." IEEE Transactions on Information Theory, Vol. 36, No. 5, September, 1990.

[64] Rioul, O., and Velterli, M. "Wavelets and Signal Processing." IEEE SP Magazine, October, 1991, pp. 14.

[66] Mallat, S.G. "Multifrequency channel decomposition of Images and Wavelet Models." IEEE Trans. Acous. Speech Signal Processing, Vol. 37, No. 12, December, 1987. pp. 2091.

[66] Tuteur, F.B. "Wavelet Transform in signal detection." IEEE Int. Conf. on Acoustics, Speech and Signal Processing, Vol. 3, 1988, pp. 1435.

[67] Daubechies, I. "Orthonormal bases of compactly supported Wavelets." Commun. Pure Appl. Math. Vol. 41, November, 1988, pp. 909.

[68] Kronland-Martient, R., "The wavelet transform for analysis, synthesis and processing of speech and music sounds." Computer Music Journal, Vol. 12, No. 4, 1988, pp. 11.

ACKNOWLEDGEMENTS

I would like to extend my appreciation to Dr. Lalita Udpa and Dr. Satish Udpa for their support and guidance throughout my master's degree program. Their insight, patience and kindness provided an excellent work environment and has truly made me proud to be a part of their team.

I would like to thank Dr. Lalita Udpa for proofreading my thesis repeatedly. I am also indebted to Dr. William Lord and Dr. H.A. David to be on my committee.

Special thanks to Micheal S. Chan for helping me with the computer simulations and to David Berry for helping me get acquainted with the project.

I would like to dedicate this work to my father, Mr. Ram Kewalram Shahani, who has always been a column of support and faith. His patience will always be remembered.

Appendix A

The back-propagation algorithm minimizes the error function E with respect to the interconnection weights. The error E is defined as

$$E = \frac{1}{2} \sum_{c} \sum_{j} (y_j - d_j)^2 \qquad \text{(A-1)}$$

where c is the case index for the output pairs, j is the index over the output units, y is the calculated output and d is the desired output. To minimize E, we find the derivative of the error with respect to each weight in the network. We start by calculating the error at the output layer and propagate the error back to the input layer.

The total input to a unit is the linear combination of the inputs and can be written as

$$x_j = \sum_{i} y_i w_{ij} \qquad \text{(A-2)}$$

where w_{ij} is the weight connecting y_i to x_j. The output of the unit can be expressed as

$$y_j = \frac{1}{1 + e^{-x_j}} \qquad \text{(A-3)}$$

The derivative of the error $\partial E / \partial w_{ij}$ can be expressed using the chain rule as

$$\frac{\partial E}{\partial w_{ij}} = \frac{\partial E}{\partial x_j}.\frac{\partial x_j}{\partial w_{ij}} \qquad \text{(A-4)}$$

Differentiating equation (A-2) yields

$$\frac{\partial x}{\partial w_{ij}} = y_i \qquad \text{(A-5)}$$

Also $\partial E/\partial x_j$ can be expressed as

$$\frac{\partial E}{\partial x_j} = \frac{\partial E}{\partial y_j}.\frac{\partial y_j}{\partial x_j} \qquad \text{(A-6)}$$

Differentiating equation (A-1) and (A-3) and combining the result with equation (A-6) yields

$$\frac{\partial E}{\partial y_j} = (y_j - d_j)(1 - y_j)\, y_j \qquad \text{(A-7)}$$

The above equation indicates how a change in the total input will affect the error. Further, the total input is a function of the states of the lower level units and weights.

For output node j

$$\frac{\partial E}{\partial w_{ij}} = \delta_j y_i \qquad \text{(A-8)}$$

where $\delta_j = (y_j - d_j)(1- y_j)y_j$

For hidden node j

$$\frac{\partial E}{\partial y_j} = \sum_k \frac{\partial E}{\partial x_k} \cdot \frac{\partial x_k}{\partial y_j} \qquad \text{(A-9)}$$

where k is over the nodes in the output layer.

$$\therefore \frac{\partial E}{\partial w_{ij}} = (1 - y_j)\, y_j \sum_k \delta_k w_{jk} \qquad \text{(A-10)}$$

In order to implement gradient descent method, the weight correction scheme calculates the gradient of the error curve and updates the interconnection weights by an amount Δw, proportional to the gradient value. This correction will move the weight values in the direction of error minimum. The incremental change in each weight is thus chosen to be proportional to the derivative of error w.r.t. the weights. i.e.

$$\Delta w = \eta \frac{\partial E}{\partial w} \quad 0 < \eta < 1 \qquad \text{(A-11)}$$

Appendix B

The discrete cosine transform (DCT) of a (Nx1) sequence given as { x(0), x(1), x(2), . . . x(N-1) } can be obtained form the discrete Fourier transform of a (2Nx1) symmetrically extended sequence of the form { x(N-1), x(N-2), . . . x(1), x(0), x(0), x(1), ... x(N-2), X(N-1) }.

Proof:

The DFT of a sequence { y[n] }, n=0,1, . .2N-1 is given as

$$Y[k] = \sum_{n=0}^{2N-1} y[n]\, e^{\frac{-j2\pi nk}{2N}} \quad , k = 0, 1, \ldots 2N-1 \qquad n = 0,1, \ldots 2N-1 \tag{B-1}$$

Splitting the summations over two intervals, we have

$$Y[k] = \sum_{n=0}^{N-1} y[n]\, e^{\frac{-j2\pi nk}{2N}} + \sum_{n=N}^{2N-1} y[n]\, e^{\frac{-j2\pi nk}{2N}} \tag{B-2}$$

where due to the symmetric extension we have

$y[n] = x[N-1-n] \quad 0<=n<=N-1$

and $y[n] = x[n-N] \quad N<=n<=2N-1$

Substituting for y[n] in equation (B-2) we have

$$Y[k] = \sum_{n=0}^{N-1} x[N-1-n]\, e^{\frac{-j2\pi nk}{2N}} + \sum_{n=N}^{2N-1} x[n-N]\, e^{\frac{-j2\pi nk}{2N}} \qquad \text{(B-3)}$$

Substituting p = N-1-n in the first summation and p= n-N in the second summation, we get

$$Y[k] = \sum_{p=0}^{N-1} x[p]\, e^{\frac{-j2\pi(N-1-p)k}{2N}} + \sum_{p=0}^{N-1} x[p]\, e^{\frac{-j2\pi(p+N)k}{2N}} \qquad \text{(B-4)}$$

Rewriting equation (B-4) we get

$$Y[k] = \sum_{p=0}^{N-1} x[p] \left\{ e^{\frac{-j2\pi(N-1-p)k}{2N}} + e^{\frac{-j2\pi(p+N)k}{2N}} \right\} \qquad \text{(B-5)}$$

Simplifying (B-5) further, we have

$$Y[k] = \sum_{p=0}^{N-1} x[p]\, e^{-j\pi k} \left\{ e^{\frac{j(p+1)2\pi k}{2N}} + e^{\frac{-j2\pi pk}{2N}} \right\} \qquad \text{(B-6)}$$

Using trigonometric identities, Y[k] can be expressed as

$$Y[k] = \sum_{p=0}^{N-1} x[p]\, e^{-j\pi k} e^{\frac{j2\pi k}{N}} \left\{ \cos[\pi(\frac{2p+1}{2N})k] \right\} \qquad \text{(B-7)}$$

Since $e^{-j\pi k} e^{\frac{j2\pi k}{N}}$ is a constant w.r.t. p, we have

$$Y[k] = e^{-j\pi k} e^{\frac{j2\pi k}{N}} \sum_{n=0}^{N-1} x[n] \left\{ \cos\left[\pi\left(\frac{2n+1}{2N}\right)k\right] \right\} \qquad \text{(B-8)}$$

which is the discrete cosine transform of a sequence { x[n] }, n =0,1,. . . N-1.